Nuclear Science
2023; 8(1): 8-29
http://www.sciencepublishinggroup.com/j/ns
doi: 10.11648/j.ns.20230801.13
ISSN: 2640-4338 (Print); ISSN: 2640-4346 (Online)

Evaluation of the Basic Neutronics and Thermal-Hydraulics for the Safety Evaluation of the Advanced Micro Reactor (AMR)

Wayne Arthur Boyes[1], Johan Slabber[2], Charl du Toit[3], Francois van Heerden[4]

[1]Department of Reactor Design, STL Nuclear (Pty) Ltd., Pretoria, South Africa

[2]Department of Mechanical and Aeronautical Engineering, University of Pretoria, Pretoria, South Africa

[3]Unit for Energy and Technology Systems, North-West University, Potchefstroom, South Africa

[4]Radiation and Reactor Theory, South African Nuclear Energy Corporation NECSA (SOC, Ltd), North-West, South Africa

Email address:

wayne.boyes@thorium100.com (Wayne Arthur Boyes), johan.slabber@up.ac.za (Johan Slabber), Jat.DuToit@nwu.ac.za (Charl du Toit), francois.vanheerden@necsa.co.za (Francois van Heerden)

To cite this article:

Wayne Arthur Boyes, Johan Slabber, Charl du Toit, Francois van Heerden. Evaluation of the Basic Neutronics and Thermal-Hydraulics for the Safety Evaluation of the Advanced Micro Reactor (AMR). *Nuclear Science*. Vol. 8, No. 1, 2023, pp. 8-29.
doi: 10.11648/j.ns.20230801.13

Received: March 28, 2023; **Accepted**: April 27, 2023; **Published**: May 10, 2023

Abstract: South Africa requires safe affordable distributed base load energy, one way to achieve this is to use nuclear power integrated with renewable energy sources on a decentralized basis. This suggests the development of its own micro modular nuclear reactor, to supply energy to towns, small communities, mines and processing plants. Large Light Water Reactors (LWRs) are expensive and require a large infrastructure development. A High Temperature Reactor (HTR) called the Advanced Micro Reactor (AMR) is in the process of being developed and the design philosophy is to design for inherent safety, maximally using technology that has been developed and validated in previous HTR programs albeit in a completely different and unique configuration. The concept is based on existing knowhow and experience/expertise in South Africa during the time of the Pebble Bed Modular reactor (PBMR) project. These AMR reactors are to be factory built to obtain good quality control and rolled out to various sites. Once the reactor has reached its end of life, it would be returned to a licensed organisation for refuelling. The AMR produces 10MW of thermal power. The reactor configuration uses hexagonal graphite blocks for structural and moderator material, which are arranged to form a cylindrical core layout. The fuel assemblies are silicon carbide tubes that house coated particle fuel, immersed in a lead-bismuth eutectic alloy (LBE). Each fuel assembly is contained in a boring within the graphite moderator that allows an annulus for cooling. There are 420 fuel assemblies in the core. Low enriched fuel in the form of UO_2 or UCO is used. Helium gas is used as coolant. The coolant enters the core at 450°C and exits at 750°C. The mechanical, neutronic and thermal-hydraulic design of the AMR, is being evaluated with assistance from STL Nuclear (Pty) Ltd., the University of Pretoria (UP), the North-West University and the South African Nuclear Energy Corporation (NECSA). The OSCAR-5 code package, together with the Serpent neutronic code were used to perform the basic neutronic studies while the Flownex package was used to determine the thermal-hydraulic and safety evaluation for the Design Base Accident (DBA) specifically the Depressurized Loss of Forced Cooling (DLOFC) event.

Keywords: Depressurized Loss of Forced Cooling (DLOFC), High Assay Low Enriched Uranium (HALEU), High Temperature Gas Reactor (HTGR), Lead Bismuth Eutectic (LBE), Silicon Carbide (SiC), TRIstructural-ISOtropic (TRISO), Uranium Oxycarbide (UCO)

1. Introduction

STL Nuclear (Pty) Ltd., the University of Pretoria, the North-West University in conjunction with the South African Nuclear Energy Corporation (NECSA) are developing a 10 MW_{th} Small Modular Reactor (SMR) called the Advanced Micro Reactor (AMR). This reactor falls in the category of

the High-Temperature, Gas Cooled Reactors (HTGRs). The AMR uses helium as the coolant and is graphite moderated. It uses graphite hexagonal blocks as the moderator and these blocks are arranged to form a cylindrical configuration. The graphite core contains 420 borings with a single silicon carbide (SiC) tube fuel assembly in each. The individual SiC fuel assemblies contain TRISO coated particles with either uranium dioxide (UO_2) or uranium oxycarbide (UCO) ceramic fuel kernels of 19.9 wt% enriched uranium. The voids between the coated particles are filled with a Lead Bismuth Eutectic (LBE) alloy to provide good heat transfer from the fuel particles to the fuel assembly wall. The outer diameter of the Reactor Pressure Vessel (RPV) is 2.78 m. Road transportability was taken into consideration in the design which limited the outer diameter of the RPV.

The reactor is designed to:

1) Have excess reactivity to operate for several years before refueling is required.
2) Enable road transportation and for making it easier to fabricate.
3) Be factory assembled to ensure good quality control.
4) Utilize proven HTR technologies albeit in a different configuration.

The AMR is shown Figure 1.

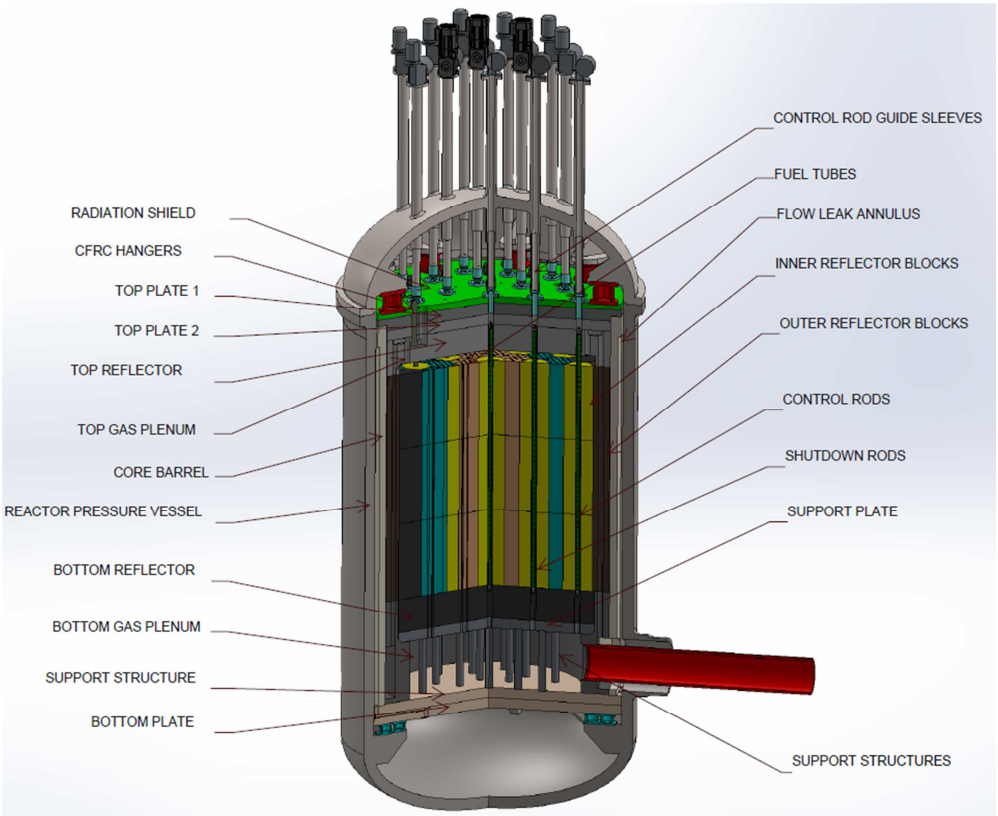

Figure 1. *AMR Reactor.*

2. The Amr Design Description

2.1. Design Characteristics

The design objectives adopted for the reactor has been taken from the guidelines developed by the Generation IV International Forum (GIF) [5] with major focus on enhanced safety, minimised waste production and proliferation resistance features.

The AMR is shown in Figure 1. The reactor is a high temperature helium-gas cooled reactor with a power of 10 MW_{th}. The helium coolant is circulated through the reactor core by an electric blower located within the pressure boundary. As is the custom for thermal neutron-spectrum high temperature reactors, graphite is used as moderator, which in this design, is in the form of hexagonal graphite blocks packed to form an approximate cylindrical configuration with a diameter and height (including radial reflectors as well as top, bottom and) respectively of ~2.2 m (~1.72 m active diameter), and 2.4 m (active length 2.2 m) with a volume of 5.103 m^3 which results in a core power density of ~1.959 MW/m^3. The fuel assemblies are silicon carbide tubes that contain the fuel in the form of low-enriched uranium (LEU) dioxide (UO_2) or uranium oxycarbide (UCO) TRIstructural-ISOtropic (TRISO) coated particles, immersed in a Lead Bismuth Eutectic (LBE) (45 % Pb and 55% Bi) alloy. The lead bismuth eutectic has very good thermal conductivity and a low coefficient of thermal expansion while being nearly transparent to neutrons [6]. The fuel assemblies are evenly spaced lengthwise in the hexagonal block graphite structures with an annulus around each for cooling by helium entering the core at the top. A graphite neutron reflector surrounds the core on the sides, top

and bottom. The reactor core design parameters are shown in Table 1.

Table 1. *Reactor core design parameters.*

	Nominal value or description	**Unit**
Thermal power	10	MW_{th}
Primary coolant	Helium	
Moderator	Graphite	
Core geometry	Hexagonal blocks forming a cylindrical layout	
Core diameter (active)	1.72	m
Core height (active)	2.200	m
Core volume	5.10	m^3
Height to dimeter ratio (H/D)	1.28 (>0.97)	
Average power density	1.959	MW_{th}/m^3
Linear Power Density $\dot{q}$ (Fuel tube)	0.017	MW/m
Core inlet temperature	450	°C
Core outlet temperature	750	°C
Coolant flow rate	6.42	kg/s
Primary coolant pressure	4	MPa

A cutaway of the reactor vessel and internal structures from Figure 1 is shown in Figure 2 where the core layout configuration can be seen.

The reactor core model is based on a conventional prismatic reactor core layout. The helium coolant enters the reactor vessel at 450°C through the annulus of the co-axial duct. The helium then flows upwards in the helium risers located in the outer graphite reflector. Helium leak flow also enters the annular space between the Core Barrel (CB) and the inside of the Reactor Pressure Vessel (RPV). The helium flow enters the top of the reactor core where it is evenly directed to the 420 borings containing the fuel assemblies as well as between the annuli of the control rod guide-tubes. The helium leak flow also enters the top and bottom RPV domes. The helium from the bottom dome re-joins the leak annulus between the CB and RPV, while the helium entering the upper dome flows past the control rod guides and metallic components and connects to the upper gas plenum and is routed downwards to join the major coolant flow past the fuel assemblies. Some helium from the upper dome is also forced into coolant holes within the control rod guide sleeves which flows in the inner anulus of the control rods, this then exits the sleeve and re-joins the major downward flow in the core. The helium then flows downward through the annulus in the borings past the fuel assemblies to remove heat and exits the core at 750°C. It is then collected in a lower core hot gas plenum that is part of the lower core support structures and flows back through a hot duct (connected to the hot gas plenum) to the Heat Pipe Heat Exchanger (HPHE).

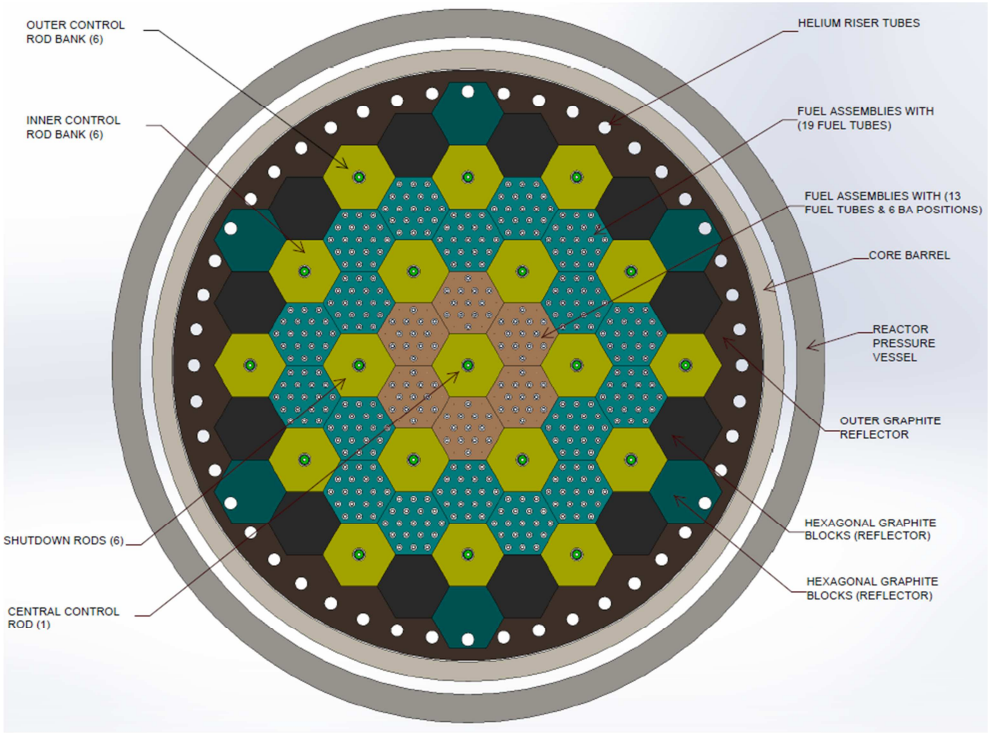

Figure 2. *AMR core layout.*

The coupled neutron physics and thermo-fluid dynamics design of the AMR reactor features three specific characteristics as described below.

2.2. Safety Requirements

The three general safety requirements that reactors have to fulfil worldwide for all postulated events are to be able to shut the reactor down, to ensure that the fuel temperature is brought down to a safe level and to avoid any activity that may be present from being released into the environment. These requirements overlaid on the AMR design can be described as follows:

1) In the event of core heat-up the relatively strong negative temperature coefficient of reactivity will always shut down the nuclear chain reaction immediately and as a defence-in-depth the two diverse shutdown systems are each capable of shutting the reactor down with fresh fuel when the reactor is cold.
2) The design can remove residual heat entirely by thermal conduction, thermal radiation, and natural convection after a postulated DLOFC event. During such an event the universally accepted temperature limit for this fuel type is 1600°C. During normal operation the maximum fuel temperature remains below 1130°C. This temperature is based on the results obtained in the German fuel testing program to ensure that no additional coated particle failures occur over and above those that were present in the fresh fuel initially. These limits are guaranteed through the design measures of the coupled neutronics and thermo-fluid dynamics behaviour within the given geometry and material selection.
3) The reactor has two barriers of SiC, that being the SiC layer surrounding each fuel kernel as well as the SiC fuel tube of the fuel assembly (see 3.2). This introduces an additional barrier which will further reduce the probability of any radioactivity being released into the environment. In addition to the two abovementioned barriers, the pressure boundary serves as a third barrier against release of radioactivity, and then as a final barrier the reactor building can also be accredited as a final enclosure.

3. Fuel and Moderator

3.1. Coated Particle Characteristics

The defining characteristic of the high temperature reactor and the key to the safety and operational simplicity of the AMR is the use of TRISO fuel particles.

Figure 3 shows the construction details of a typical coated particle. The SiC is the main layer for the retention of fission products.

Although the AMR is designed for UCO, it is not limited to the use of only UCO fuel shown in Table 2. In Germany and in the U.S., TRISO particles have been manufactured into other chemical forms, such as UO_2, or UC_2 containing other fissile isotopes of uranium and plutonium typically U-233 and Pu-239.

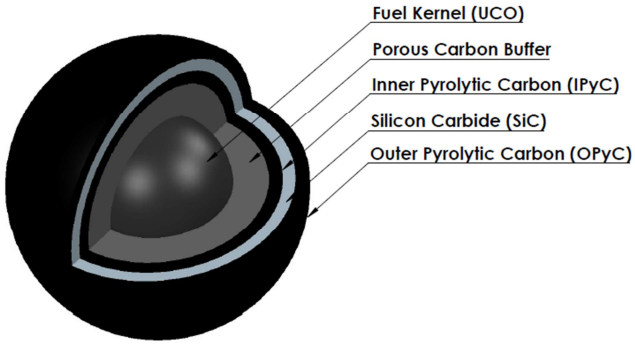

Figure 3. *Coated particle depicting multi-barrier TRISO coated particles.*

The AMR is also not only limited to kernel and coated particle diameters of 425 microns (μm) and 855 microns (μm) respectively. German standard kernel diameters of 500 microns (μm) and coated particle diameters of 920 microns (μm) can also be utilized. The AMR is not restricted to using only high assay low enriched uranium (HALEU). Simulations have been performed with enrichments of ~10 wt% to 15 wt% with good results. For the purposes of this paper, only HALEU of 19.9 wt% enriched uranium is shown.

The AMR while maintaining inherent safety characteristics, can use alternate fuels without modifications to the reactor. Advanced fuel cycles for later investigation for use in the AMR range from a (Th, U) O_2 fuel cycle using both LEU and HEU, to a UC_2 fuel cycle. This study however only reports on the analysis of the UCO composition.

Table 2. *Coated particle parameters.*

Description	Size	Unit
Fuel kernel diameter	425	μm
Kernel coating material	C/IPyC/SiC/OPyC	
Layer thickness	100/40/35/40	μm
Layer densities	1.15/1.95/3.21/1.95	g/cm^3
Fuel enrichment	19.9	wt%
Fuel type	UCO	

3.2. Fuel Assembly Characteristics

The fuel assembly is a Silicon Carbide tube with an outside diameter of 1.5 cm and a wall thickness of 0.15 cm leaving an inner diameter of 1.2 cm. Coated particles together with a heat transfer/filler material consisting of a eutectic alloy of lead and bismuth (LBE) forms the inside of the fuel assembly. The tube is manufactured with one end sealed while the open end is sealed after it is filled with the fuel LBE mixture. The length of a single fuel assembly is ~73 cm across the ends. Approximately ~463775 coated particles will be contained in a typical fuel assembly.

3.3. Moderator/Reflector Characteristics

There are four types of hexagonal blocks making up the core

structures of the AMR. These blocks are all of the same dimensions but contain a different number of borings and/or material. The blocks without any borings are called reflector blocks, blocks with a single large boring are called control rod blocks and then the blocks containing the fuel assemblies are of two types; namely blocks with 13 (this contains 6 burnable poison positions) and 19 borings respectively. Figure 4 shows an image of a block with 19 borings. The core is surrounded by solid graphite blocks and fulfils the role as neutron reflector. The graphite in all the foregoing descriptions functions as moderator although, due to its neutron scattering characteristics it predominantly scatters neutrons back towards the core and thereby is also a good neutron reflector on the outer edge of the core. Three hexagonal blocks are stacked upon one another lengthwise in the core. The borings in the fuel containing blocks have a diameter of 25 mm and with the fuel assembly centred inside these borings an annulus with thickness of 5 mm is provided flow of coolant. The main reason for using a fuel assembly of the same length as a block is to simplify quality of manufacture. Some of the fuel-containing blocks also contains in some of the borings, tubes loaded with burnable neutron absorber material for the purpose of lengthening the operational period between fuel reloading, this can be seen in Figure 5.

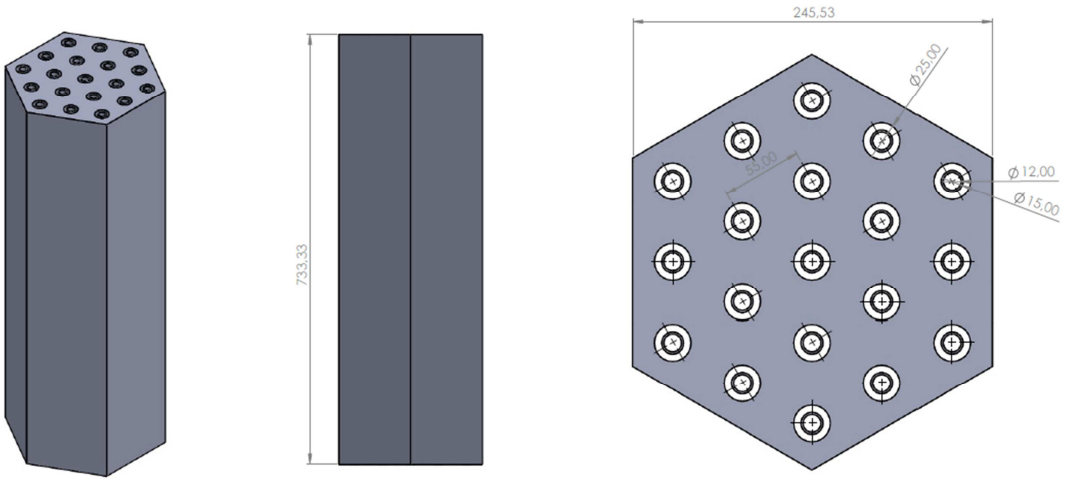

Figure 4. *AMR Fuel Block with 19 fuel positions.*

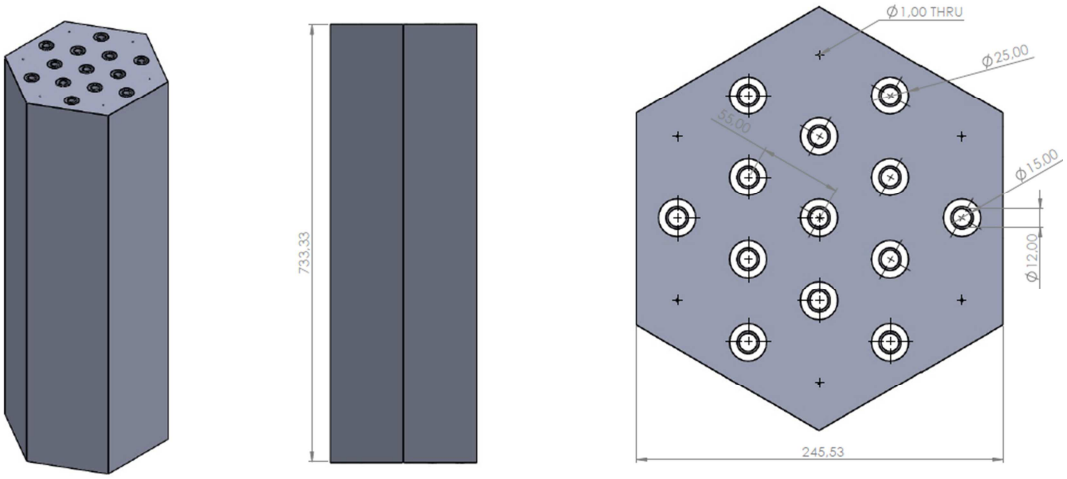

Figure 5. *Burnable Absorber Fuel Block with 13 fuel positions and 6 BA positions.*

4. Heat Pipe Heat Exchanger (HPHE)

A Heat Pipe Heat Exchanger (HPHE) is used to transfer heat from the reactor core to the secondary power conversion loop containing air. A lead bismuth eutectic (LBE) alloy is used to absorb heat from the primary helium coolant bundle (located in the central U-tube bundle) and surrounded by a flow-directing shroud. This heat is then exchanged by means of natural convection with the secondary power loop (in the form of a multiplicity of U-tubes) located in the annulus between the flow-directing shroud and the inner wall of the outer shell of the heat exchanger. The LBE returns to the central hot helium bundle at the bottom through several portals in the flow-directing shroud. This flow of LBE in this design can be described as "toroidal natural convection flow". The HPHE only demonstrates a limited number of tubes to illustrate the gas flow paths, this is shown in Figure 6 and Figure 7.

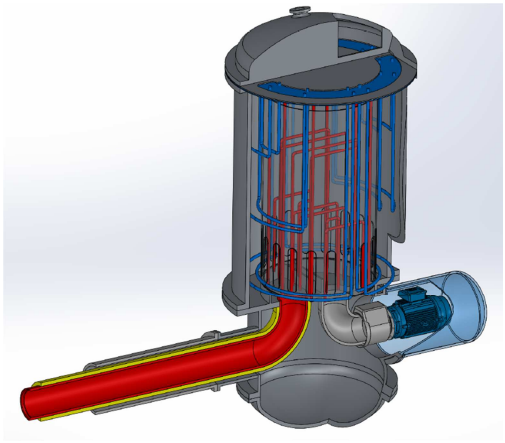

Figure 6. *Heat Pipe Heat Exchanger (HPHE) concept (demonstrating a limited number of tubes).*

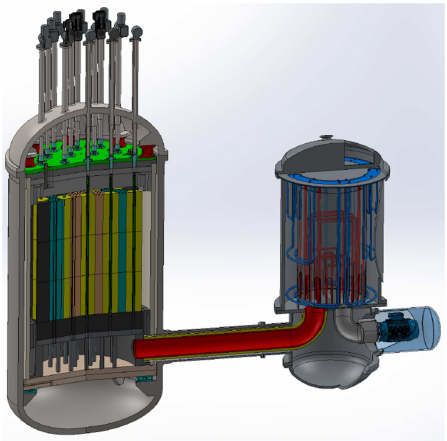

Figure 7. *Heat Pipe Heat Exchanger (HPHE) concept (limited tubes) coupled to the Advanced Micro Reactor (AMR).*

5. Safety Characteristics

The four principles of stability have been incorporated into the AMR design; these are as follows:

1) Nuclear stability – Nuclear transients may never lead to unallowable power output excursions or cause unallowable fuel temperature overheating.
2) Thermal stability – The reactor core cannot melt or overheat to a temperature where its capability to retain fission products is compromised.
3) Mechanical stability – The core may never be allowed to deform or change composition.
4) Chemical stability – Fuel assemblies may never be allowed to corrode excessively.

These design principles, taken as a design guide, resulted in the following specific characteristics:

1) Nuclear stability: If all control and shutdown systems are accidentally withdrawn, it will not lead to fuel damage or a radionuclide release. There is no requirement for active safety systems or operator action to prevent fuel damage. This is achieved with a relatively large negative temperature coefficient of reactivity over the entire operational range, a low core power density, a core geometry that will ensure passive decay heat removal and the radionuclide retention capacity of the TRi-Structural ISOtropic (TRISO) particle fuel as well as the SiC structure of the fuel assembly.

Xenon oscillations is damped due to the H/D ratio of the core of less than 3 which is normally used as guideline for inherent stability.

2) Thermal stability: The low power density is ensured in the core design as well as a high thermal capacity and height to diameter ratio (H/D) greater than 0.97 to ensure that the decay heat removal can solely be achieved through conduction, natural convection, and radiation through the reactor structures. Reutler and Lohnert [2] determined that increasing the height/diameter ratio beyond 0.97 in a trade-off between neutron losses versus the advantage of gaining passive decay heat removal via the walls of a steel pressure vessel in the event of a DLOFC [2].

A key inherent safety characteristic of typical HTR design is keeping the fuel temperatures during a DLOFC event low enough that the escape of radioactive material through the coating layers around the fuel kernels will be limited to acceptable levels. From the German fuel qualification results Pebble Bed Reactor (PBR) design philosophy is that the maximum fuel temperature during a DLOFC event should remain below the set limit of 1600°C for the dioxide-based fuel (UO_2).

The American Advanced Gas Reactor (AGR) program based on uranium oxycarbide UCO fuel kernels set the temperature limit to 1800°C. This is claimed to be due to the lower internal particle pressures due to less oxygen formation within the coated particles [1].

3) Mechanical stability: The design also ensures that the materials of construction remain below the structural design limits and the maximum fuel temperatures in an accident condition remain below the set fuel damage limits.
4) Chemical stability: The design of the core and its coolant routing is such that in an event that could allow air to leak into the pressure boundary, there is no possibility that a sustained corrosion of core components by air can take place. The reactor also does away with the possibility of a water or steam ingress scenario [3] as the helium coolant will transfer heat to a Heat Pipe Heat Exchanger (HPHE) which is a single-phase natural convection heat pipe heat exchanger using Lead Bismuth (Pb-Bi) Eutectic (LBE) as working fluid. This heat exchanger is then coupled to a Brayton power conversion cycle.

The use of a HPHE also introduces another important safety feature by eliminating the possibility of tritium, produced in the primary helium cooling circuit to contaminate the air in the secondary circuit by diffusing through a single tube wall.

This study investigates if the design of the AMR reactor and assesses the core operating at normal conditions at a Maximum Continuous Rating (MCR) of 100% power (10

MW_{th}). This will be called the equilibrium condition at 100% MCR.

The neutronics of the equilibrium core were analysed with the OSCAR-5 and SERPENT codes. The Flownex code is used to assess the thermal hydraulic behaviour of the AMR core and to assess the DLOFC event.

6. Simulation Methods and Models

6.1. The OSCAR-5 Code System

The OSCAR code suite is a nodal diffusion-based code which has been used over many years for research reactor analyses.

The OSCAR-5 system aims to allow for multi-code, multi-physics support for reactor analysis, with the primary aim to allow the use of fit-for-purpose tools in support of reactor operations. This implies finding a balance between the nature of a specific calculation application and the level of detail and fidelity utilized in achieving the result. The OSCAR-5 system is built around the concept of a code-independent, consistent reactor core model. This model is deployable to an extendable set of integrated target codes and manages the passing of data between these target codes. Currently fully coupled to the system is an in-house OSCAR nodal package, Serpent and MCNP. Figure 8 shows the OSCAR-5 system design architecture.

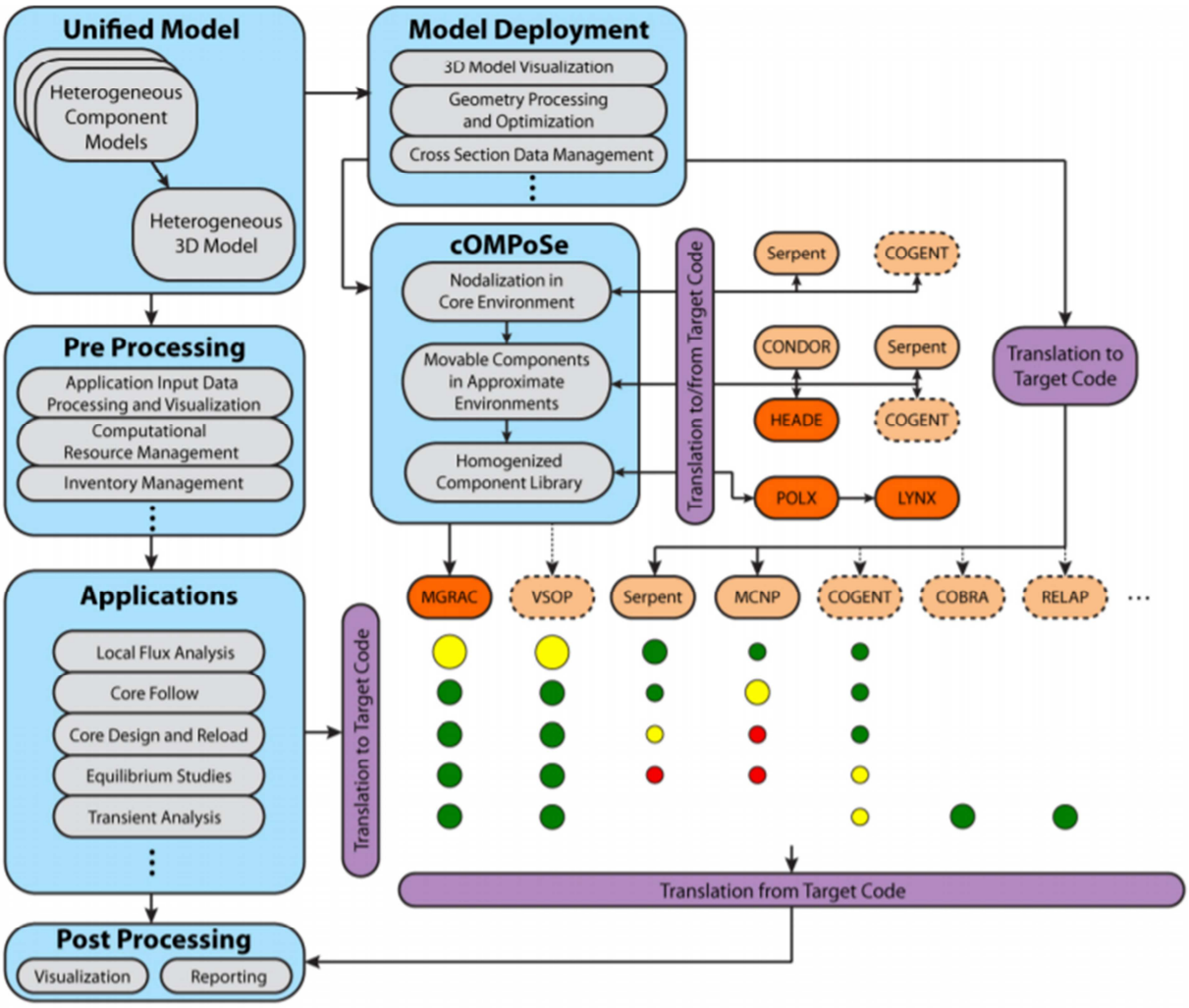

Figure 8. *OSCAR-5 system design architecture.*

6.2. The SERPENT Code System

SERPENT is a three-dimensional, continuous-energy Monte Carlo reactor physics burnup calculation code specifically designed for lattice physics applications. The code uses built-in calculation routines for generating homogenized multi-group constants for deterministic reactor simulator calculations. The standard output includes effective and infinite multiplication factors, homogenized reaction cross sections, scattering matrices, diffusion coefficients, assembly discontinuity factors, point-kinetic parameters, effective delayed neutron fractions, and precursor group decay constants. User-defined tallies can be set up for calculating various integral reaction rates and spectral quantities. Internal burnup calculation capability allows SERPENT to simulate fuel depletion as a completely stand-

alone application.

OSCAR5 is used as a pre-processing code to develop input files for SERPENT. OSCAR-5 allows for the development of the reactor model, and this is then used to generate the input file for SERPENT which then is used to simulate a finite reactor geometry for the AMR cylindrical core.

Table 3. *AMR Material Properties.*

Description	Material
Reflector graphite	Reactor Graphite, SGL, Grade A, NBG10
Static Helium Gap	Helium
Core Barrel (CB)	Stainless Steel SA-240 grade 316
Reactor Pressure Vessel (RPV)	Steel SA-508
Top/Bottom Plate	Stainless Steel SA-240 grade 316
Additional Metallic Structures	Inconel 800 H

The conventional material model for the AMR in OSCAR-5/SERPENT utilizes graphite hexagonal blocks and graphite reflectors, a core barrel, and a reactor pressure vessel [4]. Refer to Table 3 for the reactor material selections.

Furthermore, several important design features are important:

1) The hexagonal blocks, top, bottom and side reflectors consist of isotropic nuclear-grade graphite.
2) Hexagonal blocks forming an approximate cylindrical core with a total of 420 core borings each with a single SiC fuel assembly filled with coated particles and LBE. There are 18 fuel blocks (in a single layer) and 6 burnable absorber blocks (in a single layer). The fuel blocks contain 19 fuel assemblies while the burnable absorber blocks contain 13 fuel assemblies and 6 burnable poison strands.
3) The effective core height is fixed at 2.4 m and an (approximated) core diameter of 2.2 m, inclusive of the top, bottom and side reflectors.

This is shown in Figure 9.

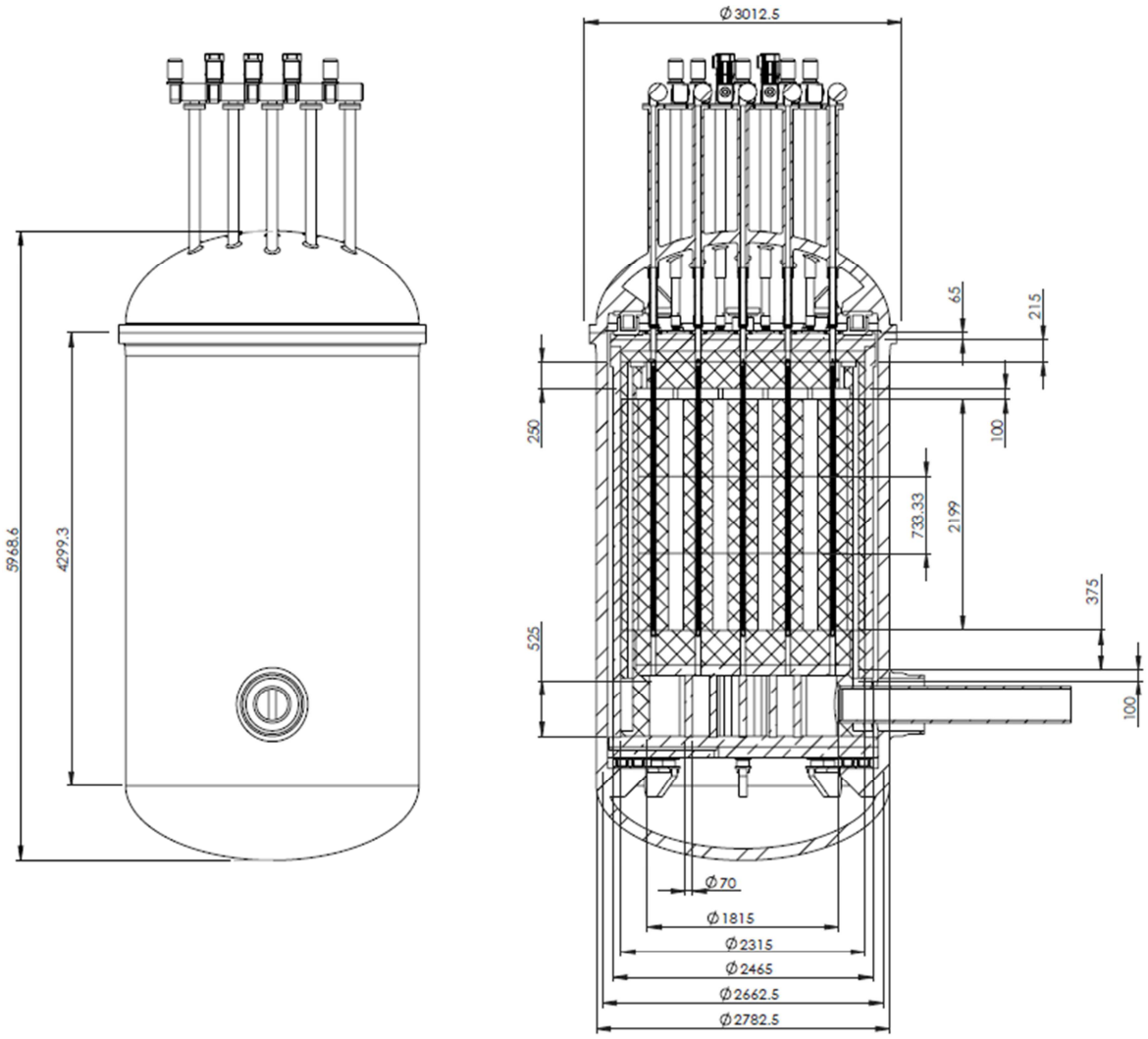

Figure 1. *AMR geometrical layout.*

7. Neutronic and Temperature Results

7.1. Pitch Optimization

As can be seen in Figure 10. the optimal centre to centre fuel tube pitch which provided the highest k_{eff} was located at ~ 75 mm between the centres of the fuel tubes. The highest k_{eff} values seem to be around the 65 mm to 85 mm mark with regards to centre to centre of the fuel assemblies which is shown in Figure 11. This is around 40 mm to 60 mm with regards to the graphite material between borings.

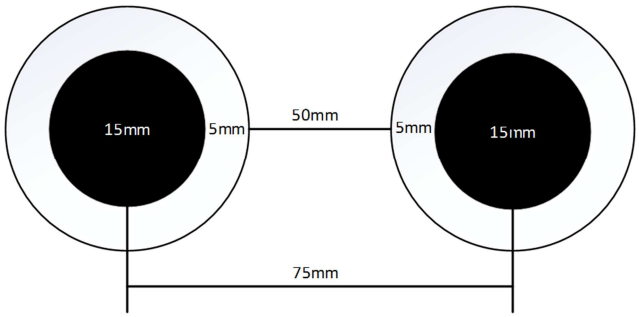

Figure 10. *Optimal centre to centre fuel pitch length.*

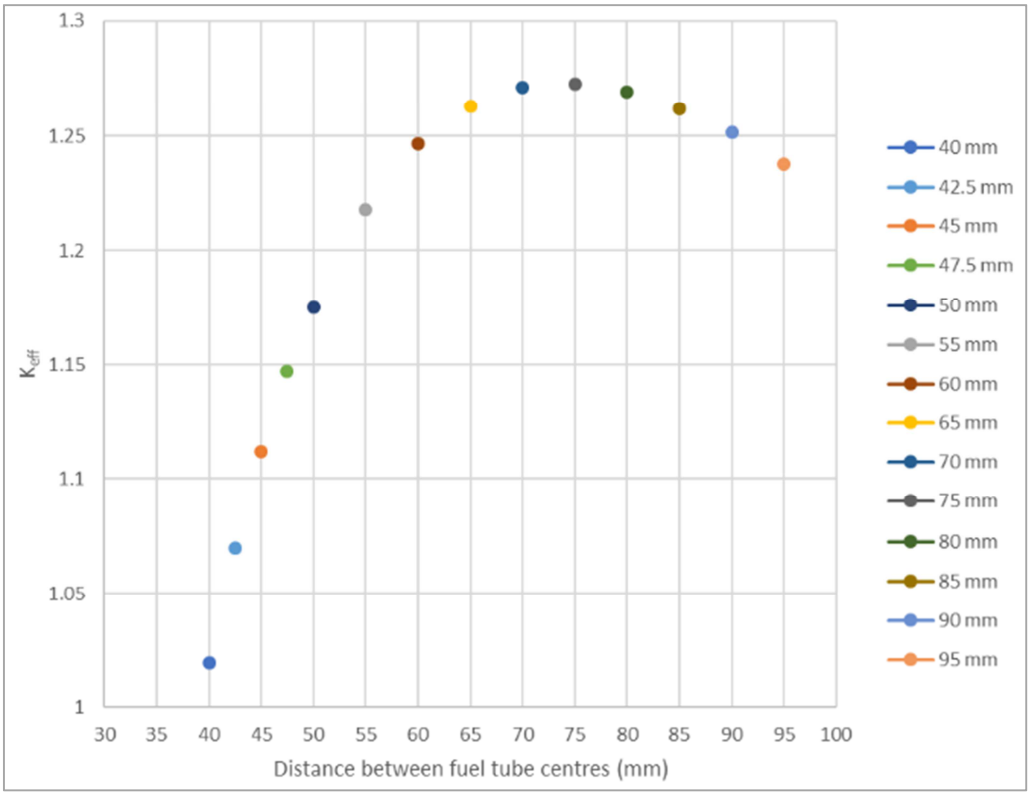

Figure 11. *Centre to centre fuel pitch distances vs k_{eff}.*

This 75 mm distance between fuel assemblies made the outer pressure vessel diameter much larger, around ~4 m which makes it much more difficult to transport, thus a more compact fuel pitch was chosen for the AMR.

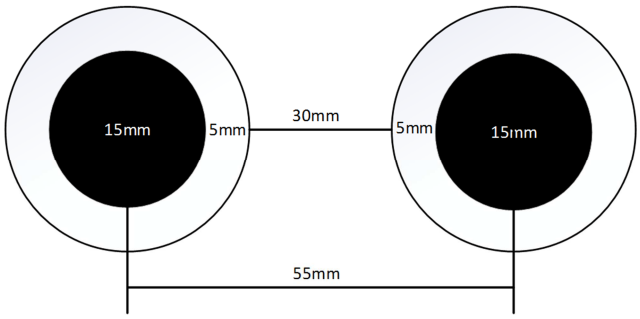

Figure 12. *Chosen centre to centre fuel pitch length.*

A pitch of 55 mm between fuel tube centres was chosen. This equates to an outer boring distance (graphitic material distance) between borings of 30 mm seen in Figure 12. Although this is not the optimum pitch this allows for the outer RPV to be transported on the road. The RPV outer diameter in this case is 2.78 m. The k_{eff} is still high which allows for excess reactivity to operate the reactor for an adequate number of years before refuelling.

7.2. Maximum Fuel Temperatures in Normal Operations

The normal operational maximum central fuel temperatures were also determined. The reactor configuration with a single assembly per boring with coated particles within a fuel assembly using two heat transfer mediums within the sealed SiC assemblies were

assessed. The first heat transfer medium to assist in heat transfer from the kernels through the SiC assembly to the outer coolant was helium and the second the Lead Bismuth Eutectic (LBE). The SiC fuel assemblies have a 15 mm outer diameter with a 1.5 mm wall thickness and an inner diameter of 12 mm and a boring diameter of 25 mm. The number of fuel assemblies and sizes of the coolant channels are shown in Table 4.

Table 4. *Fuel assemblies & coolant gap diameters.*

Core configuration	# Fuel assemblies	Coolant channel diameter
Single assembly per boring	420	25 mm

Table 5. *Maximum linear power and power density per fuel assembly.*

Core configuration	# Fuel assemblies	Max linear power density per fuel assembly (W/cm)	Max power density per fuel assembly (W/cm^3)
Single assembly per boring	420	169.91	150.236

The maximum linear power density and maximum power density per fuel assembly is shown below. A maximum to average power of 1.57 in the core was used to represent the maximum to average power ratio of the core that is shown in Table 5.

7.2.1. Coated Particle (CP) Effective Thermal Conductivity

The heat-transfer for the coated particles had to be determined. The thermal conductivity, specific heat, radiation heat transfer, thermal conductivity at coated particle contact points and effective thermal conductivity due to radiation had to be determined before the heat transfer for the two mediums was introduced. This is based on the Zehner-Schlunder correlations for the effective thermal conductivity in a pebble bed [8, 9]. This was then applied to coated particles.

The average thermal conductivity of the coated particle k_p is determined from equation 1 as the product of the individual coating layer masses multiplied by the thermal conductivity of each distinct layer; this is then divided by the total mass of a coated particle. m_i represents the mass fractions of the kernel and the 4 coating layers; m is the total mass of a kernel with its various layers and k_i represents the thermal conductivity of each layer and of the fuel kernel.

$$k_p = \sum \frac{m_i\, k_i}{m} \tag{1}$$

Thermal conductivity at coated particle contact points is shown in equation 2. k_c represents the coated particle thermal conductivity at the contact points, k_s the solid thermal conductivity, ν the fluid speed (near zero), F the force between kernels in a vertical tube, E_p is a dimensionless factor and d_p the particle diameter.

$$k_c = k_s \left(\left(\frac{3(1-\nu^2).F.d_p}{8\,E_p} \right)^{\frac{1}{3}} x\ \frac{1}{0.531} \left(\frac{1}{{d_p}^2} x \frac{d_p}{1} \right) \right) \tag{2}$$

Effective thermal conductivity due to radiation is determined from equation 3. k_r represents the effective thermal conductivity due to radiation. ε is the coated particle void fraction (porosity), β is a deformation parameter dependent on the porosity. ζ is the emissivity. k_p is the thermal conductivity of a coated particle. T_s is the temperature of the coated particles in (Kelvin). σ is the Stephen-Boltzmann constant.

$$\mathrm{k}_r = \left(\left(\left(1-(1-\varepsilon)^{\frac{1}{2}}\right)\varepsilon + \left(\frac{(1-\varepsilon)^{\frac{1}{2}}(\beta+1)}{\left(\frac{2}{\zeta s}-1\right)(\beta)} \right) \left(\frac{1}{1+\frac{1}{\left(\frac{2}{\zeta s}-1\right)\left(\frac{Kp}{4\sigma\, Ts^3 dp}\right)}} \right) \right) 4\sigma Ts^3 dp \right) \tag{3}$$

The effective thermal conductivity using the Zehner-Schlünder (ZS) correlation bed [8, 9]. k_e is the effective thermal conductivity. k_f is the fluid thermal conductivity, k_p the coated particle thermal conductivity. k is the ratio of k_f/k_p. This is shown in equations 4, 5 and 6.

$$k = \frac{k_f}{k_p} \tag{4}$$

$$k_e = k_f\left(1-\sqrt{1-\varepsilon} + \frac{2\sqrt{1-\varepsilon}}{1-k.\beta}\left(\frac{(1-k)}{(1-k\beta)^2}\ln\left(\frac{1}{k\beta}\right) - \left(\frac{\beta+1}{2} - \left(\frac{\beta-1}{1-k\beta}\right)\right)\right)\right. \tag{5}$$

$$\beta = 1.25\left(\frac{1-\varepsilon}{\varepsilon}\right)^{1.11} \tag{6}$$

7.2.2. Lead Bismuth Eutectic (LBE)

The thermal conductivity of the LBE [6] is determined from the equation 7, k_{LBE} is the thermal conductivity of the lead bismuth eutectic and T is the temperature in degrees Celsius.

The effective thermal conductivity using both interstitial helium as well as the LBE was calculated.

These equations provided an overall heat transfer within

the SiC assembly for the coated particles and the various heat transfer mediums.

The various temperatures were then determined for the central fuel kernels to the helium coolant gas on the outer side of the fuel assemblies.

$$k_{LBE} = 6.854 + 1.08\ x\ 10^{-2}\ (T + 273.15) \quad (7)$$

7.2.3. Wetted Perimeter and Helium Flow Calculations

The hydraulic diameter or flow area is determined from equation 8 [7].

$$Hydraulic\ Diameter\ (D_e) = \frac{4\ flow\ area}{wetted\ perimeter} \quad (8)$$

The mass flow rate of helium coolant for the entire core and the mass flow past each assembly was determined from equation 9 [7]. Q is the reactor power; C_p is the specific heat of the coolant gas and ΔT is the difference between the coolant outlet gas temperature and the inlet coolant gas temperature.

$$Q = mcp\Delta T \quad (9)$$

The gas properties were based on predetermined figures and on the ideal gas law in equations 10, 11 and 12. P is pressure, V is volume, n is the number of moles, R_g is the gas constant, T the temperature, ρ the density and m_g the mass flow rate of the helium gas. The formula was manipulated to determine the volumetric flow rate past the fuel assemblies.

$$PV = nR_gT \quad (10)$$

$$P = \rho RgT \quad (11)$$

$$V = \frac{m.RgT}{P} \quad (12)$$

The kinematic viscosity is determined from equation 13 by dividing the dynamic gas viscosity μ_g by the gas density ρ_g [7].

$$v_g = \frac{\mu_g}{\rho_g} \quad (13)$$

Reynolds number equation 14 is calculated by multiplying the gas density ρ_g by the velocity u_g and the hydraulic diameter D_e and dividing this by the gas viscosity μ_g [7].

$$Re = \frac{\rho_g\ u_g\ D_e}{\mu_g} \quad (14)$$

The Prandtl number in equation 15 is calculated by multiplying the specific heat C_p by the dynamic gas viscosity μ_g and dividing this by the gas thermal conductivity k_g [7].

$$\Pr = \frac{Cp\ \mu_g}{k_g} \quad (15)$$

The heat transfer coefficient h for forced convection in fully developed flow is calculated in equation 16 for the gas flowing past the fuel assemblies. The specific constant is c is multiplied by the thermal conductivity k and divided by the hydraulic diameter D_e. This is then multiplied by Reynolds number R_e and Prandtl number P_r each to their own specific power [7].

$$h = c\left(\frac{k_g}{D_e}\right) Re^{0.8} Pr^{0.4} \quad (16)$$

7.2.4. Fuel Centreline Temperatures

The generalized Fourier's correlations are used to calculate the central fuel temperatures for cylindrical co-ordinates. It is convenient to use the linear power density of the fuel rod $\dot{q}$ which is the power generated per unit length of the assembly seen in equation 17. $\ddot{q}$ is the power density and r_f is the radius of the fuel zone within the assembly [10].

$$\dot{q} \equiv \pi r_F^2 \ddot{q} \quad (17)$$

Finally, the maximum centreline coated particle fuel temperatures can be determined from the following set of equations below. The final equation incorporates equations 18, 19, 20 and 21 into the overall equation 22 to obtain the maximum fuel centreline temperature $T_{centreline}$. The gap is non-existent as the UCO/LBE mix is in contact with the SiC cladding, so equation 19 was neglected. $\dot{q}$ is the power generated per unit length of the assembly. $\ddot{q}$ is the power density and r_{fuel} is the radius of the fuel zone within the assembly. k_{fuel}, k_{gap}, k_{clad} are the thermal conductivities of the fuel, gap, and cladding. t_{gap}, t_{clad} are the thicknesses of the gap, and cladding and T_m is the bulk coolant fluid average temperature.

$$\Delta T_{fuel} = \frac{\dot{q}}{4\ \pi\ k_{fuel}} \quad (18)$$

$$\Delta T_{gap} = \frac{\dot{q}}{2\ \pi\ r_{fuel}}\ x\ \frac{t_{gap}}{k_{gap}} \quad (19)$$

$$\Delta T_{cladding} = \frac{\dot{q}}{2\ \pi\ r_{fuel}}\ x\ \frac{t_{clad}}{k_{clad}} \quad (20)$$

$$\Delta T_{surface} = \frac{\ddot{q}}{h_s} = \frac{\ddot{q}\ {r_f}^2}{2h_s(r_{fuel} + t_{clad})} = \frac{\dot{q}}{2h_s(r_{fuel} + t_{clad})} \quad (21)$$

$$T_{centerline} - T_m = \frac{\dot{q}}{2\ \pi\ r_f}\left(\frac{r_{fuel}}{2\ k_{fuel}} + \frac{t_{gap}}{k_{gap}} + \frac{t_{clad}}{k_{clad}} + \frac{r_{fuel}}{h_s(r_{fuel} + t_{clad})}\right) \quad (22)$$

The results yielded the maximum fuel centreline temperatures for both helium and LBE as a heat transfer medium within the SiC fuel assemblies for the single fuel assembly configurations.

Table 6. *Maximum fuel centerline temperatures for various heat transfer mediums.*

Core configuration	Max. fuel temperature (Helium as filler gas) (°C)	Max. fuel temperature (Lead Bismuth Eutectic as filler) (°C)
Single assembly per boring	1233.1	1101.5

Table 6 shows the maximum centreline temperatures for the helium only as well as the LBE mix. The Lead Bismuth Eutectic did lower the maximum fuel temperatures. The LBE lowered the maximum central fuel temperatures by ~130°C for the single fuel assembly per boring configuration. This has also been compared with the results obtained in Flownex. This is discussed in section 6.2.

The LBE should be used within the fuel assemblies to reduce the maximum fuel temperatures and the reduction of more than 100°C will help to reduce the maximum fuel temperatures in a Loss of Coolant Accident (LOCA) and thus provide an extra margin of safety to the design.

7.3. OSCAR-5/Serpent Equilibrium Core Results

The results presented in Table 7 are for the AMR with a single assembly per boring for the equilibrium core with no control rods inserted.

Table 7. *AMR (single assembly per boring) performance parameters at equilibrium conditions.*

Description	Unit	Value
Fuel type		UCO
Bare kernel	(μm)	425
Coated kernel	(μm)	855
Enrichment (in U-235)	wt%	19.9%
Core volume	m^3	5.2
Borings		420
Fuel assemblies		420
Coated particles per assembly		~463775
Heavy metal content per fuel assembly	g	1639 (1.639 kg)
Heavy metal loading in core	kg	688 (420 assemblies)
k_{eff}		1.25423
Power peaking factor	Qmax/Qavg	1.57
Average power per fuel assembly	W	23809
Maximum power density per fuel assembly/rod/element	W/cm^3	150.236
Linear power density per Fuel Assembly/rod/element	W/cm	169.91
Maximum fuel kernel temperature during normal operation	°C	1084 to 1101 (<1130)
Maximum fuel temperature after DLOFC event	°C	<1600
He temperature at core outlet:	°C	750

8. Flownex Simulations

8.1. General Description of the Flownex Model

The system code Flownex SE [11] was employed to construct a thermal-hydraulic network model of the AMR to simulate the thermal-hydraulic performance of the AMR for steady-state full power conditions and during a DLOFC. The reactor has been discretised into 11 rings in the radial direction. This is shown in Figure 13.

1 = Inner reflector + CR;
2 = First fuel ring;
3 = Second fuel ring (FA+CR);
4 = Third fuel ring (FA+CR);
5 = Outer reflector + CR + helium risers
6 = Gap between reflector and CB;
7 = Core barrel;
8 = Gap between CB and RPV;
9 = RPV;
10 = Cavity between RPV and Reactor Cavity Cooling System (RCCS);
11 = RCCS face plate.

In the axial direction the reactor has been discretised into 11 layers (BR = bottom reflector; LP = lower plenum; VII to I seven fuel layers, the first and last being 0.18333 m in height and the rest 0.36667 m high; UP = upper plenum; TR = top reflector). The Flownex model is divided into three networks that are inter-connected.

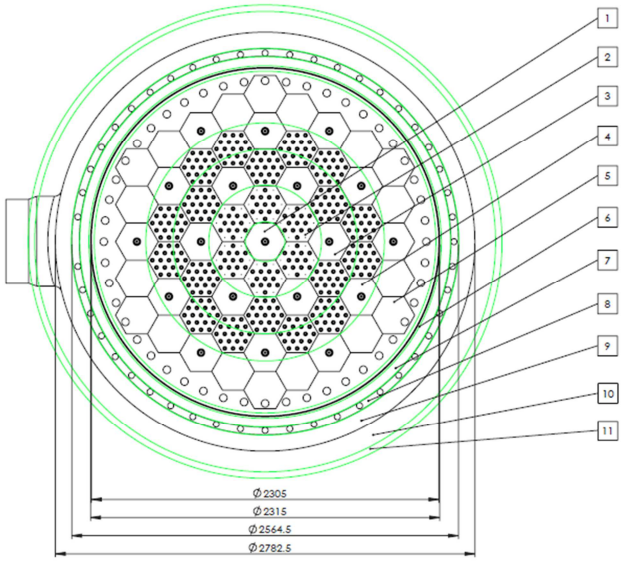

Figure 13. *AMR model showing the various radial discretized rings (cavity and RCCS not shown).*

Figure 14 shows the layout of the structures (graphite, core barrel, reactor pressure vessel, reactor cavity and RCCS face plate.

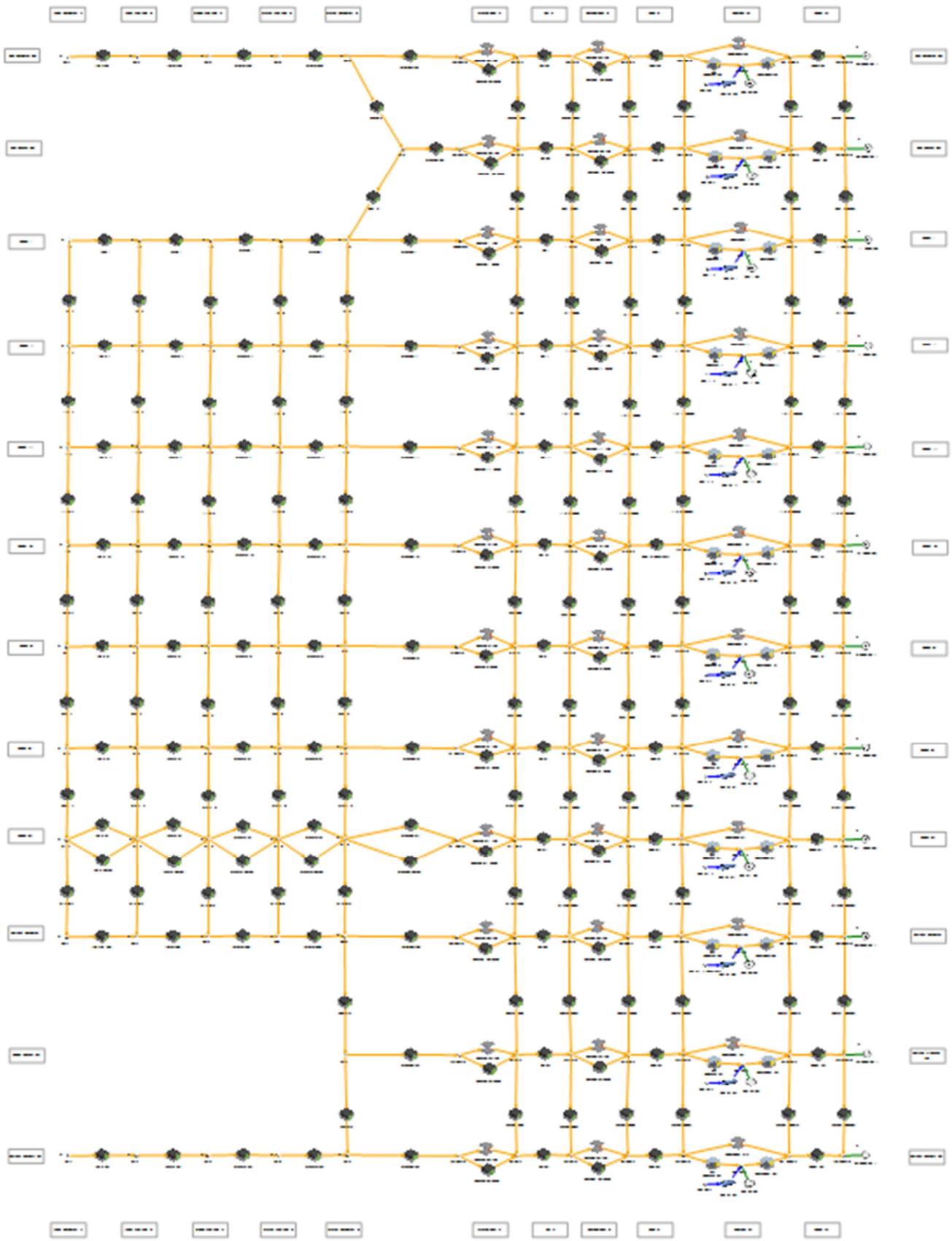

Figure 14. *Flownex structures layout of the AMR.*

Figure 15 shows the layout of the flow network which includes the control rods and the SiC tubes.

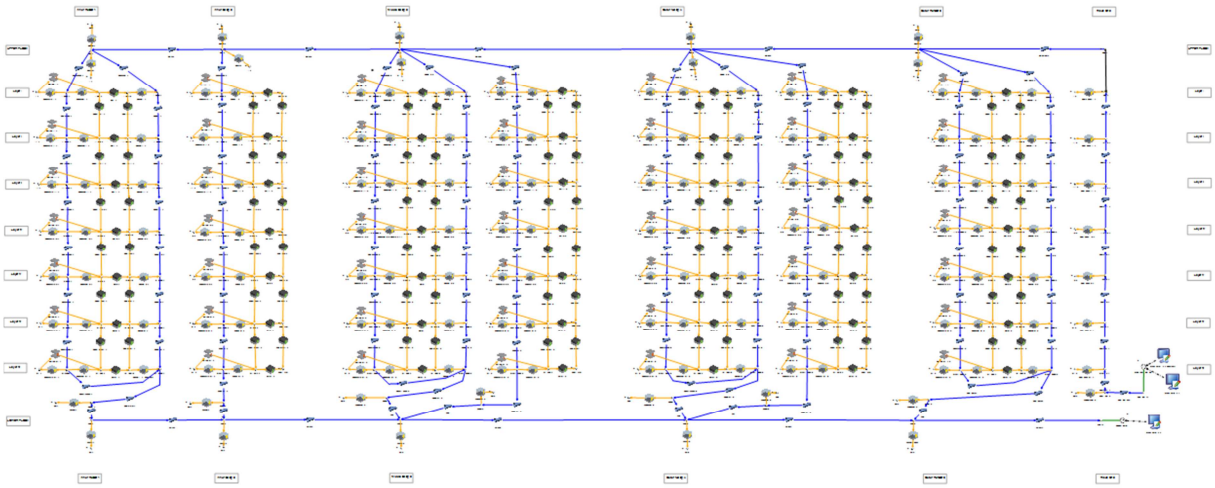

Figure 15. *Flownex flow network layout which includes control rods and SiC tubes.*

In Figure 16 the layout of the fuel network which consists of the UCO and the LBE mix inside the SiC tubes is shown.

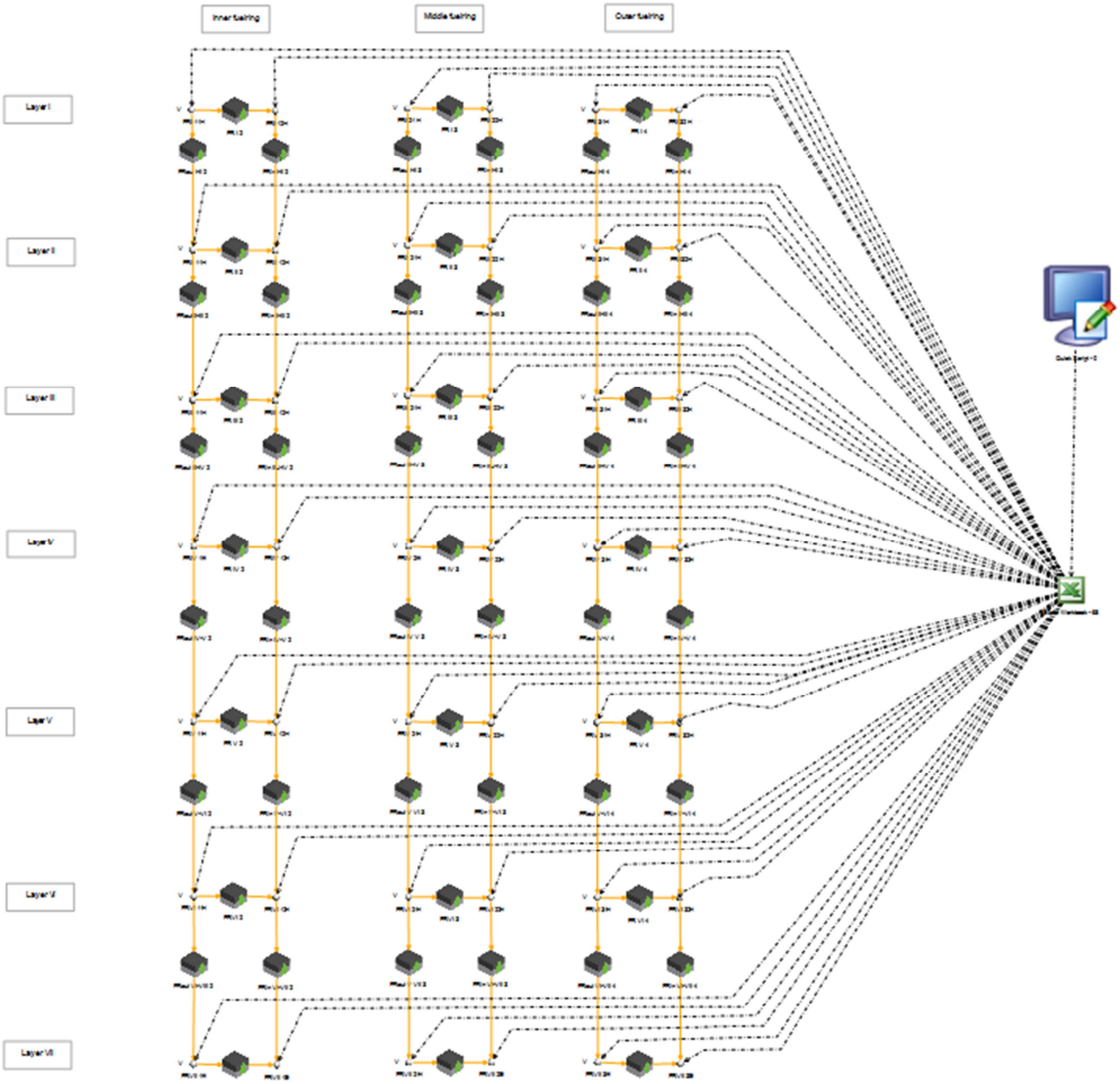

Figure 16. *Flownex layout of the fuel network consisting of the UCO and LBE mix.*

Flownex employs one-dimensional components based on a finite volume approach to account for the conduction, convection and radiation heat transfer, and the fluid flow. In the discretised rings 2 to 5 the Control Rods (CR) and fuel assemblies which is a mix of UCO coated particles, LBE and cladding [Fuel Cladding (FC) and Fuel Rod (FR)] are in each represented by an abbreviation, CR, FC and FR.

A representative Control Rod (CR) for example, has the total area and volume of the Control Rods it represents, but the conduction lengths of a single CR. This is also the case with the representative annuli which has the total flow area, wetted perimeter, and heat transfer areas of the annuli it represents, but the length and width of a single annulus.

Each graphite block is discretised into three Control Volumes (CVs) in the axial direction (quarter, half and quarter height, each with the quarter shared with that of the adjacent block, where applicable; to form a half height CV. In the radial direction each graphite block consists of one CV. The convection heat transfer component between the annuli and the graphite is thus connected to the central node of the block. The CB, RPV and RCCS face plates are all discretised into two CVs in the radial direction.

At the cold inlet of the helium flow into the reactor at a temperature of 450°C and a pressure of 4 MPa, whilst at the hot outlet of the helium a mass flow rate of 6.42 kg/s exiting the reactor was prescribed. Following Lommers et al. [19] a temperature of 65°C was prescribed on the outer surface of the RCCS face plate.

Convection heat transfer coefficients of 4.0 W/m^2.K were applied to the cavity surfaces of the RPV and RCCS face plate whilst the air in the cavity was modelled to be stagnant. The emissivities of all the surfaces were assumed to 0.8.

8.2. Flownex Steady State Results

Figure 17 to Figure 19 present the various fuel and material temperatures shown for both the elevation of the various layers within the reactor, and the associated radial positions during steady state conditions.

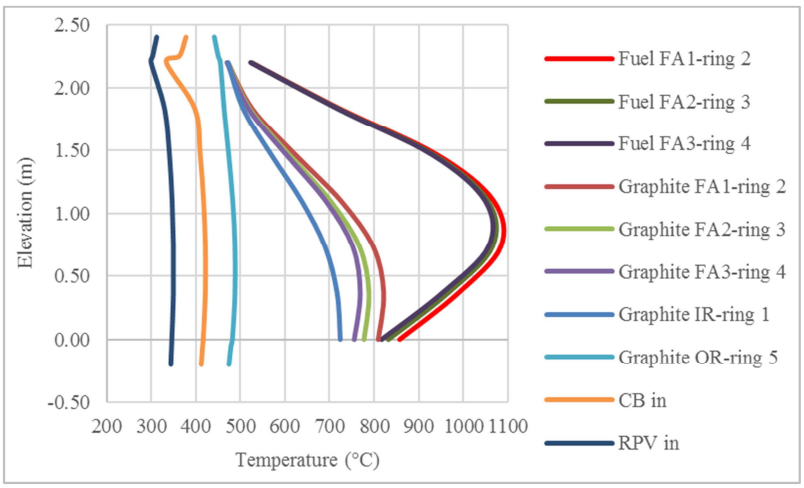

Figure 17. *Axial Temperature Variations of Various Materials and Fuel Zones at Steady-State Conditions.*

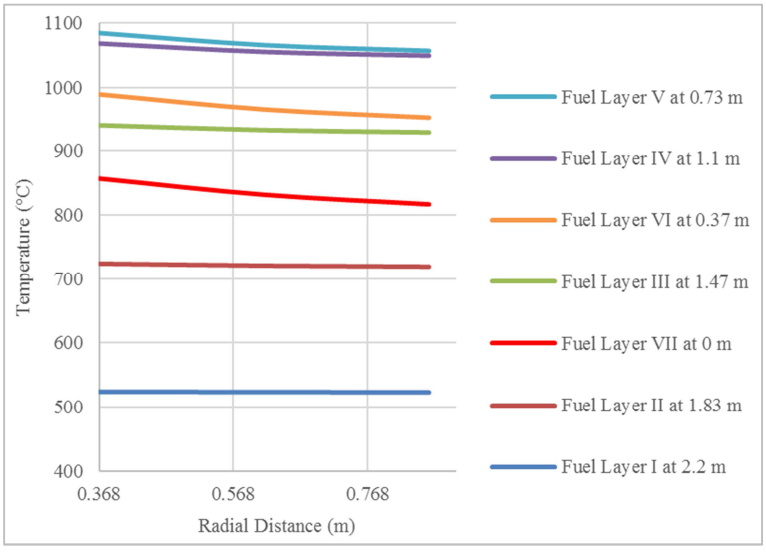

Figure 18. *Radial Temperature Variations for Various Layered Fuel Sections in the AMR.*

Figure 17 shows the axial variations of the temperatures of the various material and fuel zones at steady-state conditions. As can be seen in Figure 17 the fuel exhibits the highest temperatures with the hottest fuel being within ring 2 (the first fuel ring located nearest the centre of the core). Fuel ring 4 has the lowest maximum temperatures, this is located furthest from the core centre. The graphite follows the same trend with the graphite in ring 2 exhibiting the highest temperature and the graphite in ring 1 having the lowest apart from the reflector graphite. The other materials such as the Core Barrel (CB) and Reactor pressure Vessel (RPV) reduce in temperature as the distance away from the centre of the core increase. All materials remain within their operational structural temperature limits. The temperatures of the Inner Reflector (IR) (first ring) are less than the temperatures of the graphite of the second ring. Because no heat is generated in the IR, the heat to be transported by the helium flow associated with Control Rod (CR 1) must be conducted from the second ring requiring a positive radial temperature gradient. The remainder of the structures exhibit a negative radial temperature gradient for the heat to be transported to the riser flow and the RCCS.

The radial variations of the temperature for the various layered fuel sections in the AMR are shown in Figure 18. As can be seen the hottest fuel is located towards the central bottom part of the core located in level V at 0.73 m from the bottom of the lowest fuel layer. This is due to the fact that a sine power profile with the maximum at the centre height of the core has been applied, as well as the fact that the helium flows from the top of the core downwards thus moving the hot zone from the centre of the core to a lower level located more toward the bottom of the core. The lower fuel temperatures are located towards the top of the core. The maximum central fuel temperature being 1084.07°C within layer V. This is on par with the calculated maximum central fuel temperature value of 1101.5°C, which is only a difference of around ~17.5°C translating to a 1.6% difference. In the hand calculations it is assumed that all the coolant flows in the annuli around the fuel assemblies, radiation heat transfer across the gap between the tube and the graphite is neglected as well as the heat transfer between the graphite and the coolant. This could account for the increased maximum fuel temperature in the hand calculations compared to that of Flownex. In Flownex the Gnielinski correlation is selected to calculate the Nusselt numbers required to obtain the heat transfer coefficients.

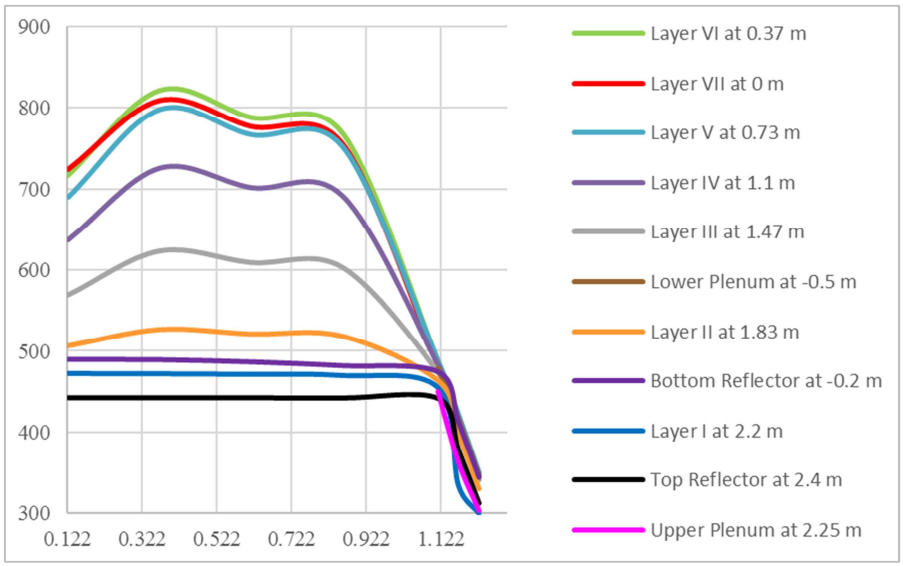

Figure 19. *Radial Temperature Variations for Various Layered Material Sections in the AMR.*

Figure 19 shows the radial variations of the temperatures of the various layered materials sections in the AMR. This provides a radial heat profile from the centre of the core outwards. The fuel layers are shown in Figure 18. above for the various elevations (layers) from the centre outwards.

It is found that 0.9%, 4.8%, 4.8% and 5.3% of the coolant flows through the CR channels in the IR, second fuel ring and third fuel ring respectively. Furthermore, it is found that 15.5%, 22.8% and 45.9% of the coolant flows through the fuel assembly channels of the first, second and third fuel rings respectively.

Lastly, it is noted that the 119.6 kW is rejected/removed by the RCCS.

8.3. Depressurized Loss of Forced Cooling (DLOFC) Transient Results

The decay heat was calculated using the correlation [12].

$$Q = 10000 \times 0.06 \times (t^{-0.2} - (t + t_0)^{-0.2}) \text{ kW} \quad (23)$$

Where t_0 is time in seconds after 15 years of operation. The mass flow rate is reduced from 6.42 kg/s to 0.01 kg/s using the same correlation and the inlet pressure is reduced from 4000 kPa to 103 kPa in the same way.

It has been found that there is virtually no change between the heat rejected by the RCCS after 360000 s

compared to the heat rejected under steady-state conditions. Furthermore, it can be shown that for t > 690 s the decay heat generated is less than heat rejected by the RCCS.

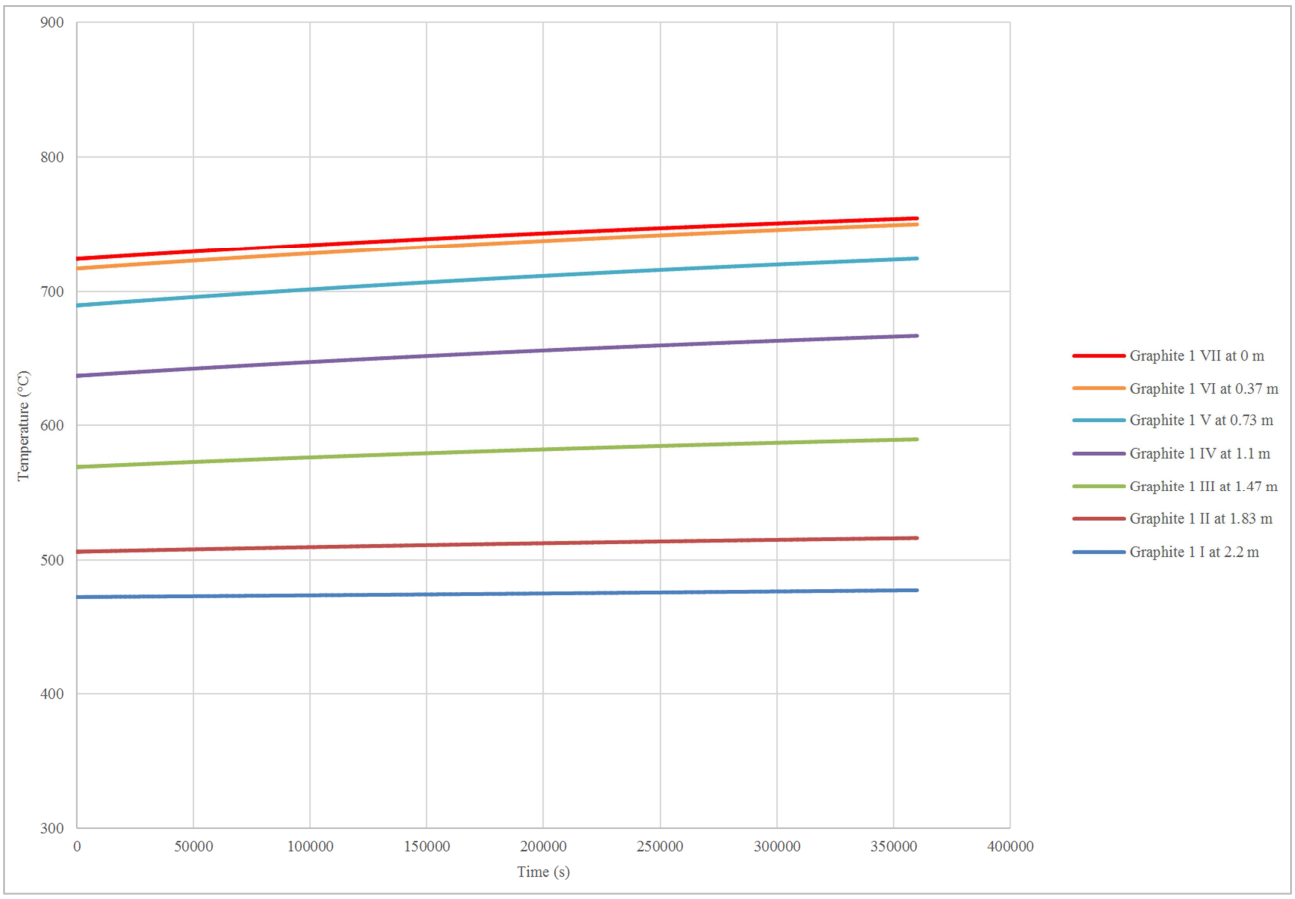

Figure 20. *Graphite zone 1 (inner reflector) temperature changes for various elevations in a DLOFC transient.*

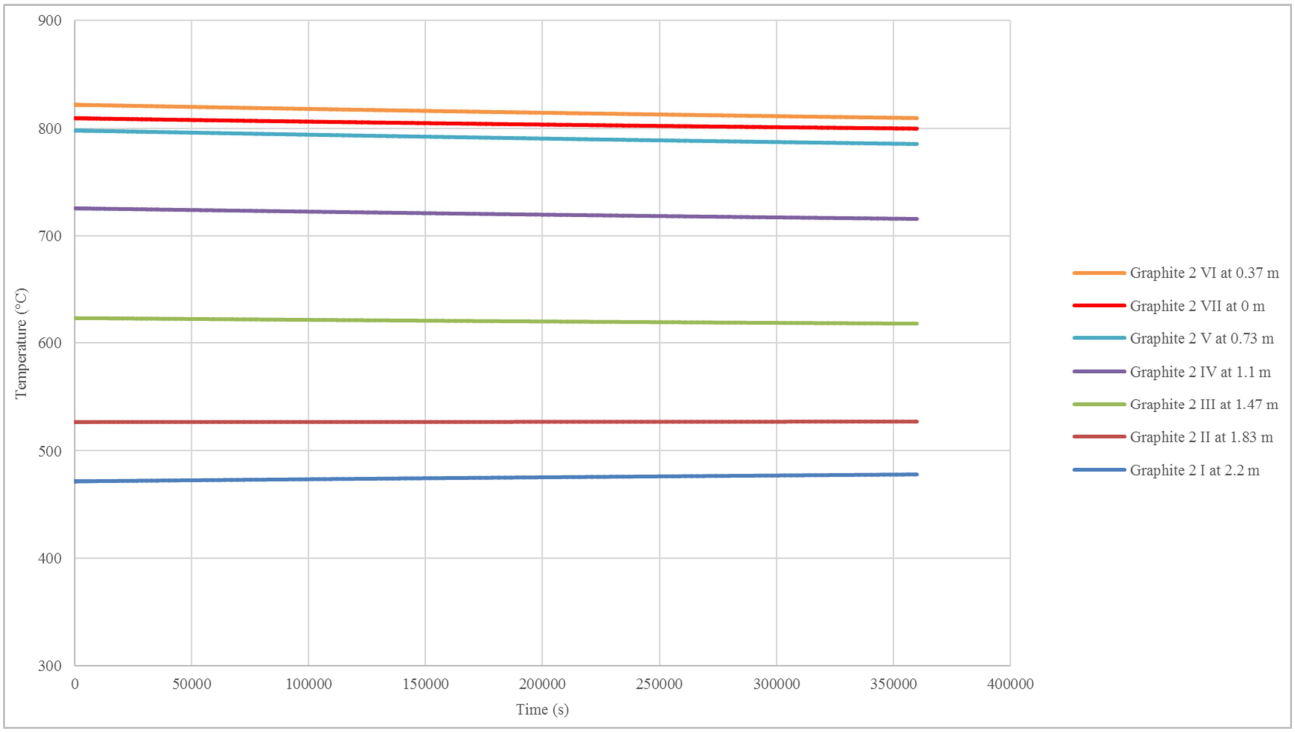

Figure 21. *Graphite zone 2 (hottest graphite) temperature changes for various elevations in a DLOFC transient.*

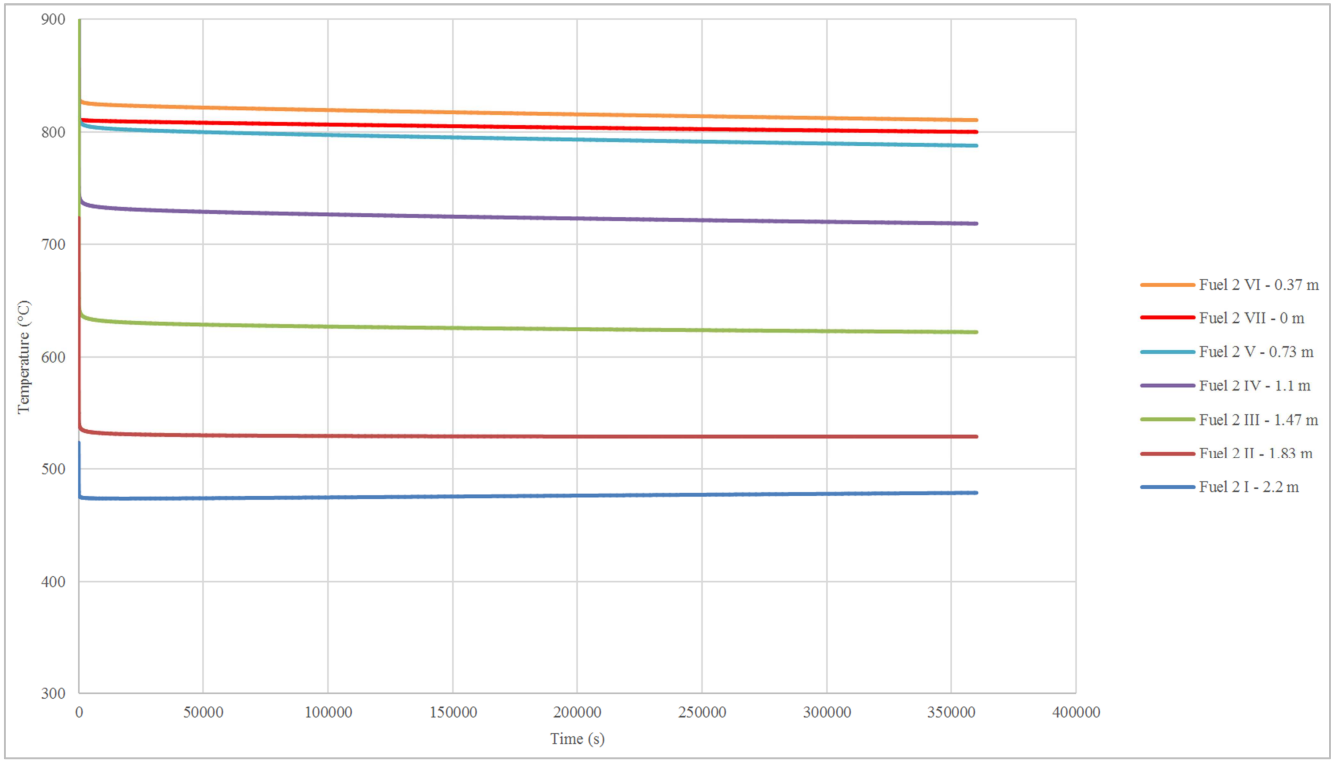

Figure 22. *Fuel zone 2 (hottest fuel) temperature change for various elevations in a DLOFC transient.*

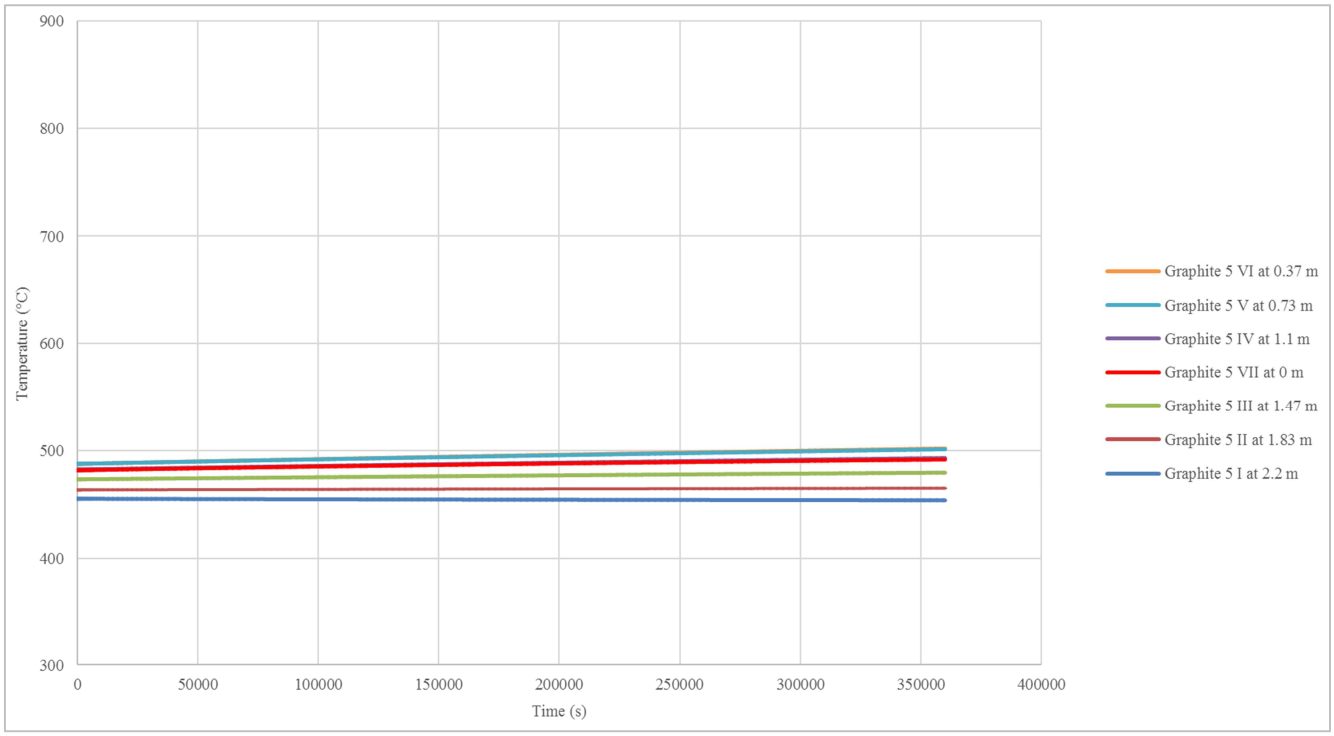

Figure 23. *Graphite zone 5 (reflector) temperature changes for various elevations in a DLOFC transient.*

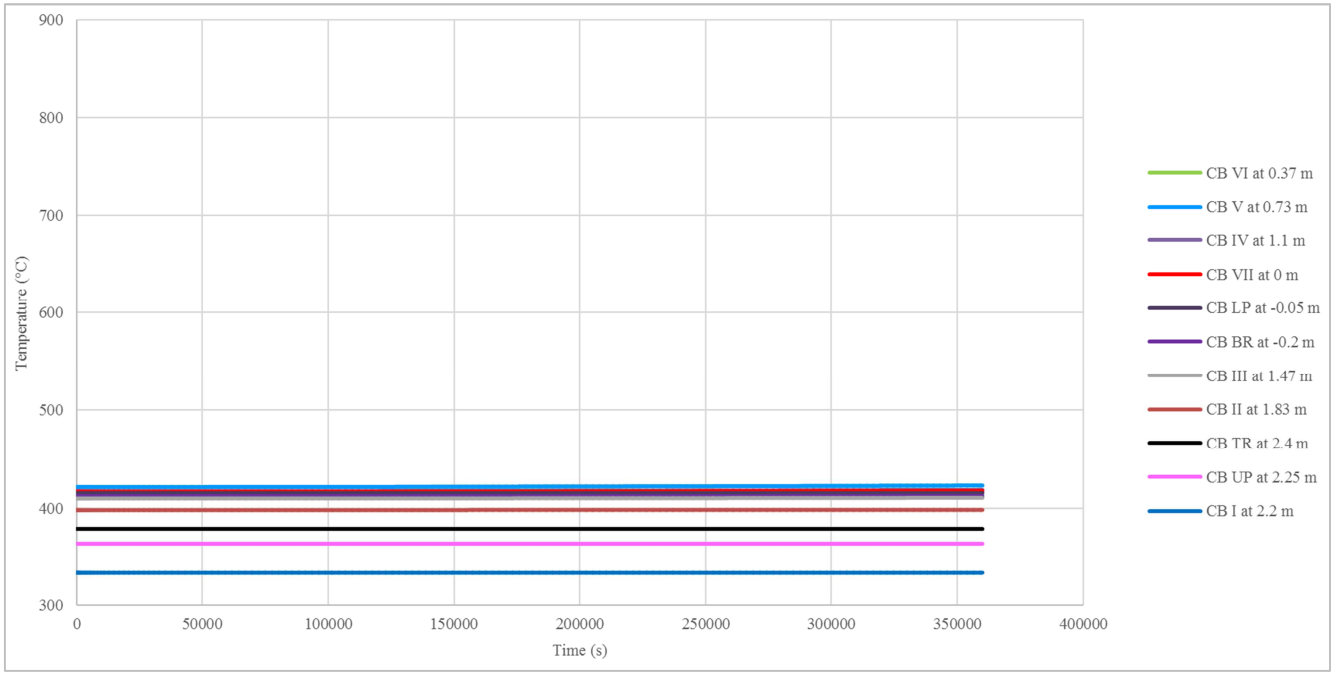

Figure 24. *Core Barrel (CB) temperature changes for various elevations in a DLOFC transient.*

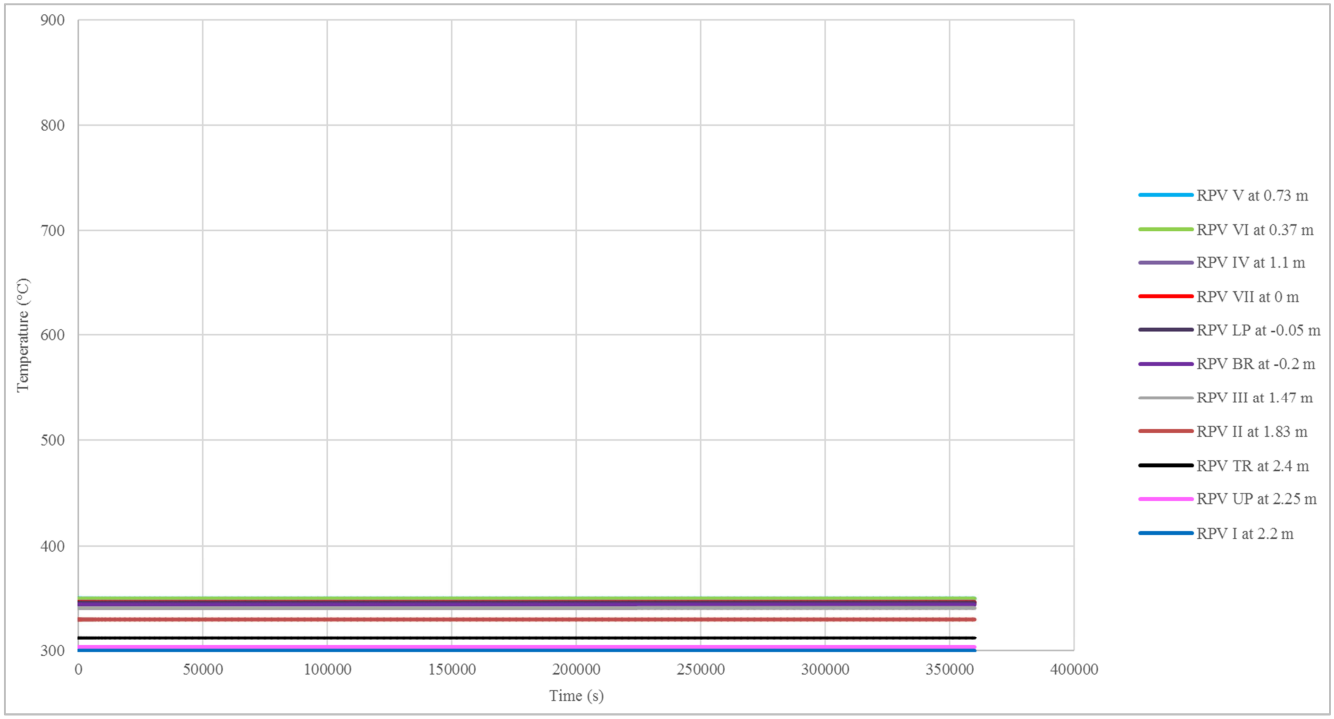

Figure 25. *Reactor Pressure Vessel (RPV) temperature changes for various elevations in a DLOFC transient.*

The temperature variation of the graphite in rings 1, 2 and 5 as a function of time are shown in Figure 20, Figure 21 and Figure 23 respectively.

The maximum fuel central temperatures in ring 2 as a function of time are shown in Figure 22. The inner surfaces for the CB and RPV as a function of time are shown in Figure 24, and Figure 25.

The variation in time of the fuel centre temperatures of ring 2 in Figure 22. shows the initial sharp drop in temperatures after the shutdown, after which most of the temperatures remain almost constant. No temperatures excursions occur as typically found in larger gas-cooled reactors.

It can be seen in Figure 20 that the graphite in ring 1 heats up because very little heat is removed by the flow in the Control Rod (CR) annulus. The heat for the temperature rise is provided by the graphite in ring 2 in Figure 21. which cools down.

Once the graphite in ring 1 has heated up sufficiently it will cool down along with the other graphite through the heat rejected by the RCCS.

The temperatures of the graphite in ring 3 (not shown) have remained relatively constant. However, the graphite in ring 4 (not shown) is cooling down to supply the heat required for the temperature rises of the graphite in ring 5 in Figure 23.

Table 8. *Temperature differences between steady state and end of transient DLOFC (100 hour) results.*

Level	Height	Graphite Temperatures				
		Graphite IR ring 1	Graphite FA1 ring 2	Graphite FA2 ring 3	Graphite FA3 ring 4	Graphite OR ring 5
	[m]	[°C]	[°C]	[°C]	[°C]	[°C]
Top Reflector at 2.4 m	2.4000	-0.013	-0.008	-0.003	-0.005	-0.136
Upper Plenum at 2.25 m	2.2500	0.000	0.000	0.000	0.000	-0.837
Layer I at 2.2 m	2.2000	5.032	6.375	5.735	3.010	-1.421
Layer II at 1.83 m	1.8333	10.026	0.452	1.851	-5.589	1.569
Layer III at 1.47 m	1.4667	20.257	-5.045	-0.657	-16.797	6.120
Layer IV at 1.1 m	1.1000	29.701	-9.682	-2.514	-27.235	10.465
Layer V at 0.73 m	0.7333	34.365	-12.253	-3.604	-33.751	13.352
Layer VI at 0.37 m	0.3667	32.980	-12.108	-3.763	-34.992	14.097
Layer VII at 0 m	0.0000	30.303	-9.448	-2.032	-32.574	9.916
Lower Plenum at -0.5 m	-0.0500					5.668
Bottom Reflector at -0.2 m	-0.2000	0.161	-0.093	-0.077	-0.055	0.698

Table 8. *Continued.*

Level	Fuel Centre Temperatures			CB	RPV	RCCS Heat		
	Fuel FA1 ring 2	Fuel FA2 ring 3	Fuel FA3 ring 4	ring 7	ring 9	Radiation	Conv	Total
	[°C]	[°C]	[°C]	[°C]	[°C]	[kW]	[kW]	[kW/m]
Top Reflector at 2.4 m				-0.002	0.000	0.000	0.000	0.000
Upper Plenum at 2.25 m				-0.012	0.000	0.000	0.000	0.000
Layer I at 2.2 m	-44.798	-45.621	-49.321	0.001	0.000	0.000	0.000	0.000
Layer II at 1.83 m	-194.334	-195.323	-203.86	0.176	0.004	0.000	0.000	0.000
Layer III at 1.47 m	-319.580	-321.776	-340.35	0.687	0.015	0.001	0.000	0.001
Layer IV at 1.1 m	-348.976	-352.454	-381.45	1.180	0.026	0.001	0.000	0.001
Layer V at 0.73 m	-296.051	-299.382	-335.41	1.509	0.034	0.001	0.000	0.001
Layer VI at 0.37 m	-178.518	-179.801	-217.77	1.595	0.036	0.001	0.000	0.001
Layer VII at 0 m	-56.949	-56.050	-93.244	1.118	0.025	0.000	0.000	0.000
Lower Plenum at -0.5 m				0.136	0.003	0.000	0.000	0.000
Bottom Reflector at -0.2 m				0.006	0.000	0.000	0.000	0.000

The relevant changes from the steady state to the results at t = 360000 s are summarised in Table 8. It is seen in Table 8 that the temperatures of the graphite in ring 1 have increased, those in ring 2 have decreased, those in ring 3 have remained almost the same, those in ring 4 have decreased and those in ring 5 have increased. The temperatures of the CB have also increased slightly. The temperatures of the RPV are virtually unchanged. The temperatures of the fuel centres in rings 2, 3 and 4 have also dropped significantly. The decay heat generated at 360000 s is 24.5 kW. The heat removed by the coolant at 360000 s is 10.88 kW. This means that 24.5 kW of the decay heat along with 95.1 kW of the heat stored in the structures is rejected by the RCCS at that point in time.

8.4. Flownex Conclusions

Based on the results it can be concluded that the integrity of the fuel will not be compromised. All materials remain within their operational structural temperature limits.

9. Conclusions and Recommendations

The preliminary neutronic and basic thermal hydraulic design of the AMR reactor was assessed. The study shows that the reactor core is feasible and can be operated for a number of years due to the high excess reactivity. A detailed burn-in of the core is still to be done.

The single assembly per boring yielded good neutronic results and best coolant gas distribution due to the uniform anulus around each fuel assembly. A pitch of 55 mm between fuel tube centres was chosen. Although this is not the optimum pitch this allows for the outer RPV to be road transportable. The RPV outer diameter in this case is 2.782 m.

The basic thermal-hydraulic calculations show the maximum fuel temperatures for the hand calculations was 1101.5°C and the maximum central fuel temperatures for Flownex being 1084.07°C (a difference of only ~17.5°C) which is 1.6%, this shows a good correlation between the two calculation methods. LBE should be used as a filler material in the fuel assembly due to the fact that it reduces the central fuel temperature by ~130°C compared to a fuel assembly only containing helium as the filler material, this greatly reduces the maximum fuel temperatures in accident conditions. The fuel will remain below the normal operational temperature guideline chosen of 1130°C and in the case of a DLOFC event will remain below the German set temperature limit of 1600°C. The fuel being used is UCO

fuel and the upper set limit of 1800°C will not be exceeded. The LBE is recommended as a heat transfer medium in the fuel assembly and should be used in the design moving forward.

The recommended work that is still to be done to be able to apply the special applications of known technology is the SiC tube development, the HPHE using LBE as heat transfer medium, the sealing of the SiC tubes including the LBE within the tubes. The neutronics still requires a full core burn-up calculation, a reactivity vs control rod position to obtain the point kinetics for Flownex Nuclear code package. Flownex Nuclear is still to be used to assess the safety case of the reactor and to couple the neutronic/thermal-hydraulics model to the HPHE and secondary power cycle.

Nomenclature

mi: Mass fractions of the individual coating layers of a coated particle (g)

m: Mass of a coated particle (g)

mg: Mass flow rate of the helium gas (kg/s)

ki: Thermal conductivity of the individual layers of a coated particle (W/m. K)

kp: Overall thermal conductivity of a coated particle (W/m. K)

kc: Thermal conductivity of the contact points between coated particles (W/m. K)

ks: Solid thermal conductivity (W/m. K)

kr: Effective thermal conductivity due to radiation (W/m. K)

ke: Effective thermal conductivity (W/m. K)

kf: Fluid thermal conductivity (W/m. K)

k: Ratio of kf/kp (dimensionless)

kLBE: Thermal conductivity of the Lead Bismuth Eutectic (W/m. K)

ν: Fluid speed of filler between coated particles (m/s)

F: Force between coated particles in a vertical tube (N/m^2)

Ep: Factor (dimensionless)

dp: Size of a particle (m)

ε: Coated particle void fraction (porosity) (dimensionless)

β: Deformation parameter dependent of porosity (dimensionless)

ζ: Emissivity (dimensionless)

Ts: Temperature of the coated particles (K)

σ: the Stephen-Boltzmann constant ($W/m^2. K^4$)

De: Hydraulic Diameter (m)

Q: Reactor power (W)

Cp: Specific Heat (J/kg. K)

Tm: Average temperature of coolant gas (K)

P: Pressure of coolant gas (KPa)

V: Volume of coolant gas (m^3/s)

n: Number of moles (mol)

Rg: Ideal gas constant (J/k. mol)

ρg: Density coolant gas (kg/ m^3)

μg: Dynamic viscosity coolant gas (kg/m. s)

νg: Kinematic viscosity coolant gas (m^2/s)

ug: Mass flow of coolant gas (m/s)

Re: Reynolds number (dimensionless)

Pr: Prandtl number (dimensionless)

kg: Thermal conductivity coolant gas (W/m. K)

$\dot{q}$: Power generated per unit length of the assembly (W/m)

$\ddot{q}$: Power Density (W/m^3)

rfuel: Radius of the fuel zone (m)

Tcentreline: Maximum temperature of the centreline fuel temperature (K)

tgap: Thicknesses of the gap (m)

tclad: Thicknesses of cladding (m)

kfuel: Thermal conductivity of the fuel (same as effective thermal conductivity ke (W/m.K)

kgap: Thermal conductivity of the gap (W/m. K)

kclad: Thermal conductivity of the SiC cladding (W/m. K)

Acknowledgements

The authors hereby wish to acknowledge the contributing members of the Radiation & Reactor Theory (RRT) Group at NECSA, the STL Nuclear neutronics and thermal-hydraulics department, the University of Pretoria, the North-West University, the Computer Aided Designer (CAD)/Mechanical Designer that all that participated in the, mechanical design, multi-physics, multi-scale coupled core neutronics and thermo-fluid dynamics design of the AMR reactor.

References

[1] Petti, D. Implications of Results from the Advanced Gas Reactor Fuel Development and Qualification Program on Licensing of Modular HTGRs. HTR 2014.

[2] G. H. Lohnert and H. Reutler "The Advantages of going Modular in HTRs", Nucl. Eng. & Des. Vol. 78, Issue 2, p. 129-136, 1 Apr. 1984.

[3] Lohnert G. H. The consequences of water ingress into the primary circuit of an HTR-Modul - From the design basis accident to hypothetical postulates. Nuclear Engineering and Design, 134 (North Holland), 159-176, 1992.

[4] Hansen, U. The V. S. O. P. System Present Worth Fuel Cycle Calculation Methods and Codes, KPD. In Dragon Project Report 915. Winfrith: Pergamon Press, 1975.

[5] Generation International Forum (Generation IV Goals 2020).

[6] Handbook on Lead-bismuth Eutectic Alloy and Lead Properties, Materials Compatibility, Thermal-hydraulics and Technologies (2015 Edition), Nuclear Energy Agency Organisation for Economic Co-Operation and Development. OECD 2015. NEA. No. 7268, 2015.

[7] Cengel, Y. A., & Ghajar, A. J. Heat and mass transfer: Fundamentals and applications (5th edition.). McGraw-Hill Professional, 2014.

[8] Zehner, P. Schlünder, E.-U. Wärmeleitfähigkeit von Schüttungen bei mässigen Temperaturen, Chemie-Ingenieur-Technik 42, 933–941, 1970.

[9] Zehner, P. Schlünder, E.-U. Einfluss der Wärmestrahlung und des Druckes auf den Wärmetransport in nicht, 1995.

[10] Slabber, J. F. M, Reactor Coolant Flow and Heat Transfer, MUA782, Department of Mechanical and Aeronautical Engineering University Of Pretoria, 2021.

[11] M-Tech Industrial, Flownex SE Version 8.14.0.4675, http://www.flownex.com, 2022.

[12] Lommers, L. J., Mays, B. E, Shahrokhi, F. Passive heat removal impact on AREVA HTR design, Nuclear Engineering and Design 271, 569-577, 2014.

.